BSGF - Earth Sciences Bulletin 2022, 193, 14
© M. Motus *et al.*, Published by EDP Sciences 2022
https://doi.org/10.1051/bsgf/2022013

Available online at:
www.bsgf.fr

OPEN ACCESS

Evolution of rift-related cover-basement decoupling revealed by brecciation processes in the eastern Pyrenees

Martin Motus[1,*], Elise Nardin[1], Frédéric Mouthereau[1,2] and Yoann Denèle[1]

[1] Géosciences Environnement Toulouse, Université de Toulouse, CNRS, IRD, UPS, CNES, 31400 Toulouse, France
[2] Université de Pau et des Pays de l'Adour, E2S UPPA, CNRS, Total, LFCR, Pau, France

Received: 3 December 2021 / Published online: 30 August 2022

Abstract – Breccias associated with tectonic, fluid and sedimentary evolution of rifted margins can provide information on a variety of processes reflecting the modes of extension. In this paper, we analyse the numerous breccias exposed in the Agly Massif that was part of the European side of the Cretaceous rift now inverted in the eastern Pyrenees. Using a combination of petrologic and sedimentologic analyses, field-based structural study, and multivariate analysis of clast shape and diversity, binding lithology and size, and breccia fabrics, we distinguish 5 types of breccias reflecting depositional, tectonic, and salt-related processes. The integration of these processes in the tectonic history of the eastern Pyrenees confirms the attribution of these breccias to the Cretaceous rifting. We emphasize the major role played by the evaporitic Triassic particularly during the first stages of rifting as a major decoupling level at the basement/cover interface. Salt tectonics and shearing assisted by the circulation of fluids are reflected by hydrofracturing at the base of the Mesozoic cover. As this weak mechanical layer is later extracted as extension increases, a brittle detachment system developed along the cover-basement interface to exhume of deep crust and mantle. The relationships between brecciation and Cretaceous extension in the Pyrenees argue for a mixed mode of rifting associated with ductile and brittle deformation during the formation of the hyper-extended rift domain.

Keywords: rifting / Pyrenees / breccia / salt-tectonics / uncoupling / detachment

Résumé – Évolution d'un système de décollement syn-rift sur une interface socle-couverture : processus de formation de brèches dans la Zone Nord-Pyrénéenne orientale. Les brèches associées à l'évolution tectonique, sédimentaire et fluide des systèmes de rifts sont des marqueurs d'une variété de processus qui reflètent les modes d'extension. Dans ce papier, nous présentons une analyse des différentes brèches du Massif de l'Agly qui appartient à la partie européenne du rift crétacé inversé dans les Pyrénées Orientales. Cette étude pluridisciplinaire combine des données sédimentologiques, pétrologiques, structurales ainsi qu'une analyse statistique intégrant les formes et diversité des clastes, les lithologies et granulométrie du liant et la fabrique des brèches. Nous distinguons 5 types de brèches qui reflètent des processus sédimentaires et tectoniques, et la remobilisation des niveaux évaporitiques. L'intégration de ces processus dans l'histoire tectonique des Pyrénées Orientales confirme la formation de ces différentes brèches durant l'épisode de rifting crétacé. Nous mettons ainsi en évidence le rôle majeur des évaporites du Trias qui jouent le rôle de niveau de décollement aux interfaces socle/couverture durant les phases précoces du rifting. La tectonique salifère et le cisaillement sur ces interfaces socle/couverture, assistés par les circulations fluides sont exprimés par les nombreuses évidences de fracturation hydraulique à la base de la couverture mésozoïque. Avec l'augmentation de l'extension, ce niveau faible mécaniquement est extrait, entraînant la formation d'un système de détachement à comportement fragile. L'évolution de ce détachement préférentiellement localisé au niveau des interfaces socle/couverture, conduit à l'exhumation de la croûte profonde et du manteau. Les relations entre les processus de formation des brèches et l'extension crétacée mettent en évidence un mode de rifting dominé par un régime mixte à la fois cassante et ductile au cours de la formation des domaines hyper-étirées du rift pyrénéen.

Mots clés : rifting / Pyrénées / brèches / tectonique salifère / découplage / détachement

*Corresponding author: mn.motus@gmail.com

1 Introduction

Lithospheric thinning at rifted continental margins is recorded by the tectonic denudation of crustal and mantle rocks in the footwall of extensional ductile or brittle shear zones, and the formation of marginal sedimentary basins. Syn-rift tectonic features may be simply preserved as "pure" *in situ* tectonic and hydraulic breccias or reworked as syn-rift tectono-sedimentary breccias in marginal basins. Syn-rift sedimentary breccias may also reveal erosion and dismantlement of normal fault scarps (Leeder and Gawthorpe, 1987; Gawthorpe and Leeder, 2000; Ribes *et al.*, 2019) or detachment systems (Friedmann and Burbank, 1995). Where evaporites are present in rift basins and mobile during crustal thinning, another category of breccias are solution-collapse breccias linked to the dissolution of evaporites (Friedman, 1997; Eliassen and Talbot, 2005). The diversity of brecciation processes is closely linked to the modes of extension (high-angle crustal-scale faulting *vs.* low-angle extensional detachment faulting involving the basement or not), fluid overpressures, diapirism, and salt tectonics. Breccias therefore arguably provide important clues to understanding the tectono-sedimentary evolution of rift systems. However, brecciation processes occur typically offshore and are therefore accessible for geological study only in a few exposed rifted margins. Here, we focus on Mesozoic basins exposed in the northern Pyrenees that constitute a unique field area where rift-related brecciations processes can be studied. During the Triassic, thick Triassic evaporites were deposited on the rift domains now inverted in the Pyrenees. Along with most of Western Europe (Ortí *et al.*, 2017), this period reflects an early stage of distributed extension associated with the Alpine orogenic cycle (*e.g.*, Angrand *et al.*, 2020). Since the concepts of crustal hyper-extension and sub-continental mantle exhumation were applied in the North Pyrenean Zone (NPZ) (Lagabrielle and Bodinier, 2008; Jammes *et al.*, 2009; Lagabrielle *et al.*, 2010), the role of salt tectonics during rifting and inversion has been emphasized as a major element of the Pyrenean rift evolution based on numerical experiments (*e.g.*, Grool *et al.*, 2019; Duretz *et al.*, 2019; Jourdon *et al.*, 2020) and field studies (Jammes *et al.*, 2010; Lagabrielle *et al.*, 2020). Despite this important effort, the temporal and spatial relationships between the basement-cover decoupling in the Triassic evaporites and mantle exhumation during rifting are not yet fully understood.

To date, the formation of breccias in or near the base of early Cretaceous extensional basins in the Pyrenees have been attributed to: (i) debris flows reworking footwall rocks of high-angle normal fault scarps (Souquet *et al.*, 1985; Debroas, 1990, 1987) or low-angle detachment systems (Jammes *et al.*, 2009; Masini *et al.*, 2014), (ii) dissolution-collapse brecciation processes during pre- and syn-rift salt mobilization (Canérot and Lenoble, 1993; Canérot *et al.*, 2005, 2004; Labaume and Teixell, 2020), (iii) hydraulic fracturing and dolomitization caused by rift-related fluid activities (Salardon *et al.*, 2017; Incerpi *et al.*, 2020b), (iv) fluid-assisted (brines) tectonic brecciations along extensional decollement localized in the Triassic evaporites and the pre-rift limestones (Clerc *et al.*, 2015, 2016; Lagabrielle *et al.*, 2020; Mukonzo *et al.*, 2020) or found in association with ultramafic rocks (Clerc *et al.*, 2012; de Saint Blanquat *et al.*, 2016; Lagabrielle *et al.*, 2016, 2019a, 2019b; Asti *et al.*, 2019), (v) *in situ* top-basement cataclastic breccias across low-angle detachment fault (Masini *et al.*, 2014; Cadenas *et al.*, 2021). These studies are based on observations made at different locations along the strike of the Pyrenean rift and therefore are valuable only at a given rift segment. Moreover, there were not designed to address specifically the question regarding the spatio-temporal evolution and position of breccias during the formation of rift-related Mesozoic basins. Here we focus on the North Pyrenean Zone of eastern Pyrenees, in the region of the Agly Massif where breccias are observed but their interpretation is controversial. We provide first a detailed description of the different types of breccias that are then integrated into a spatial and temporal evolution scheme of the Pyrenean rift.

2 The North Pyrenean Zone and brecciation processes in the Pyrenees

The Pyrenees (Fig. 1a) are part of the broad orogenic domain of Western Europe that resulted from the inversion of the Atlantic and the Tethyan rifts during the Cenozoic convergence of Africa relative to Eurasia (Angrand and Mouthereau, 2021; Mouthereau *et al.*, 2021). Collision in the Pyrenees initiated in the Late Cretaceous (Santonian) by the tectonic inversion of the European and Iberian parts of a mature rift system and ended in the early Miocene (Choukroune, 1989; Roure *et al.*, 1989; Choukroune *et al.*, 1990; Muñoz, 1992; Teixell, 1998; Beaumont *et al.*, 2000; Mouthereau *et al.*, 2014; Teixell *et al.*, 2016). They are shaped by two opposite vergent thrust belts, the South Pyrenean Zone and the North Pyrenean Zone (NPZ), and a basement core, the Axial Zone (Fig. 1a). The NPZ is a 20–40 km wide fold-and-thrust belt that preserves structures and stratigraphy of the European rift as thick and variably metamorphosed pre-rift and syn-rift Mesozoic sedimentary rocks overlying a Paleozoic basement (North Pyrenean massifs, Arize, Trois-Seigneurs, Agly among others). The NPZ is bounded to the south by the North Pyrenean Fault (NPF) in the vicinity of which are exposed km-scale bodies of subcontinental lherzolites. In a narrow band located to the north of the NPF, the sedimentary cover is affected by high-temperature/low-pressure metamorphism. Metamorphic conditions reveal temperatures up to 600 °C for pressures from 0.5 to 3–4 kbar and high geothermal gradients of 70–80 °C/km that have been acquired between 110 Ma and 85 Ma, synchronous with Cretaceous extension and alkaline volcanism (Ravier, 1959; Azambre and Rossy, 1976; Albarède and Michard-Vitrac, 1978a, 1978b; Bernus-Maury, 1984; Golberg *et al.*, 1986; Montigny *et al.*, 1986; Golberg and Maluski, 1988; Thiébaut *et al.*, 1988; Dauteuil and Ricou, 1989; Golberg and Leyreloup, 1990; Clerc and Lagabrielle, 2014; Vacherat *et al.*, 2014; Clerc *et al.*, 2015; Chelalou *et al.*, 2016; Ducoux *et al.*, 2021). North of this domain, time–temperature histories inferred from thermal modelling fission-track and (U–Th)/He analyses on zircon and apatite on granite and gneiss of the North Pyrenean massifs (Arize, Trois-Seigneurs, Agly) reveal cooling below peak temperatures of 450–350 °C at 130–100 Ma (Late Aptian-Albian: Vacherat *et al.*, 2016; Ternois *et al.*, 2019). This is interpreted to reflect denudation in the footwall of basement

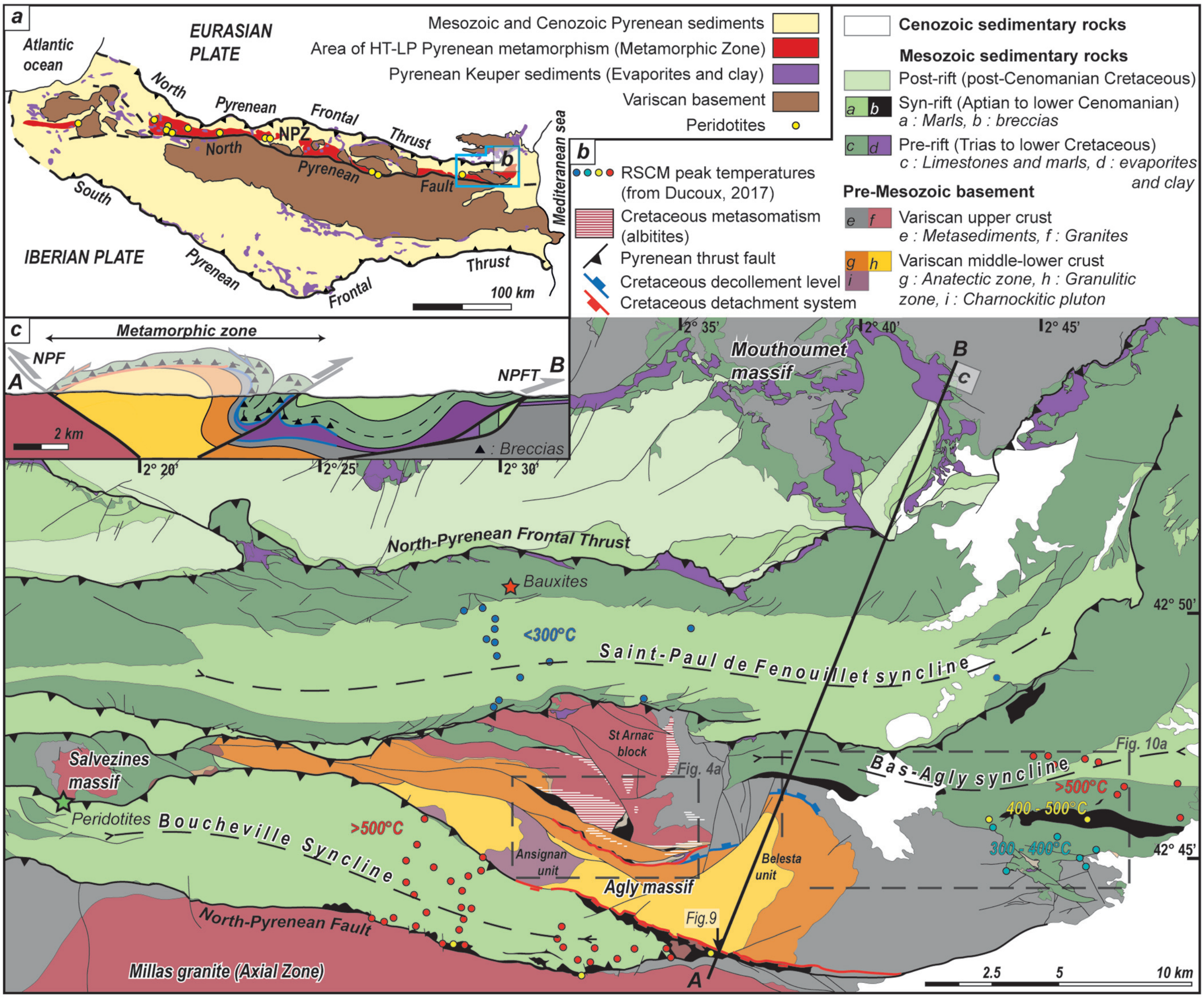

Fig. 1. Geological map of the Agly Massif and north-eastern Pyrenees. a) Simplified geological map of the Pyrenean belt. b) Geological map of the Eastern NPZ after Fonteilles *et al.* (1993), Delay (1989) and our own field mapping. c) SSW-NNE cross-section of the Agly region (see location on the geological map), no vertical exaggeration.

Fig. 1. *Cartes géologiques du Massif de l'Agly et de la Zone Nord-Pyrénéenne. a) Carte simplifiée de la chaîne des Pyrénées. b) Carte géologique de la Zone Nord-Pyrénéenne orientale d'après Fonteilles et al. (1993), Delay (1989) et notre propre travail cartographique. c) Coupe orientée SSW-NNE suivant le tracé localisé sur la carte b.*

normal faults bounding these massifs during the Cretaceous extension. In contrast, rapid cooling down below a temperature of 250–300 °C is reported during the same interval in the granulites exposed in the Agly Massif, indicating significant crustal thinning (Odlum and Stockli, 2019) in agreement with exhumation of sub-continental mantle (*e.g.*, Vauchez *et al.*, 2013). Slow cooling below 200 °C reported in the NPZ at 75–70 Ma marks the onset of inversion of the European half-rift (Mouthereau *et al.*, 2014; Ternois *et al.*, 2019, 2021; Al Reda *et al.*, 2021). A marked increase of cooling from 50 Ma records the onset of accretion of less stretched and more buoyant parts of the European half-rift domains (proximal and necking zone) at the origin of the mature collision stage in the Pyrenees (Vacherat *et al.*, 2014, 2016; Jourdon *et al.*, 2019; Ternois *et al.*, 2019, 2021; Mouthereau *et al.*, 2021).

The stratigraphy of the Mesozoic cover is represented by pre-rift Jurassic to Lower Cretaceous limestones and marls overlain by Aptian clayey limestones topped by syn-rift Albo-Cenomanian black flyschs (Peybernès and Souquet, 1984; Debroas, 1985, 1990; Souquet *et al.*, 1985). The Upper Triassic Keuper evaporite layer (Fig. 1a) plays the role of a decollement level during the Mesozoic extension and Cenozoic inversion. Its initial pre-rift thickness and distribution are not precisely known because of post-depositional tectonic movement and salt tectonics during rifting (Canérot and Lenoble, 1993; Canérot and James, 1999; Canérot *et al.*, 2005; Jammes *et al.*, 2010; Teixell *et al.*, 2016; Duretz *et al.*, 2019; Labaume and Teixell, 2020; Lagabrielle *et al.*, 2020; Ford and Vergés, 2021; Labaume and Teixell, 2020) and Pyrenean shortening (Grool *et al.*, 2019; Jourdon *et al.*, 2020; Labaume and Teixell, 2020).

Despite these uncertainties, the initial evaporite thickness is often considered to vary from a few hundred meters to kilometers (Ortí *et al.*, 2017).

Although there is no synthetic work on breccias recognized in the NPZ, many studies make a clear link between their occurrence and extension. Early works on the syn-rift basins of the NPZ revealed significant lateral facies variations within the black flysch, including polygenic breccias at the basin edges. These breccias that occasionally rework both the basement rocks and the Mesozoic cover are interpreted as sedimentary breccias formed on the slopes of normal fault scarps (Souquet *et al.*, 1985; Debroas, 1987, 1990). Another category of breccias takes the form of interbedded chaotic masses often found associated with occurrences of authigenic quartz crystals in their matrix that indicate a close relationship with upper Triassic evaporites. They are interpreted to result from syn-rift diapirism and dissolution-collapse processes (Canérot and Lenoble, 1993; Canérot *et al.*, 2005, 2004; Labaume and Teixell, 2020).

Breccias that consist of a polymictic association of metamorphosed and foliated Mesozoic clasts with ultramafic fragments, are documented in the vicinity of the Lherz peridotite body in the Aulus basin (central NPZ) (Clerc *et al.*, 2012). This type of breccias recognized in several places in central and western NPZ is interpreted as formed by tectonic-sedimentary processes reworking the Mesozoic cover (hangingwall) and the sub-continental peridotites (footwall) of an extensional detachment formed in the distal domain of the rift (Jammes *et al.*, 2009; Clerc *et al.*, 2012; de Saint Blanquat *et al.*, 2016; Lagabrielle *et al.*, 2016). Tectonic-sedimentary breccias reworking granulites have also been identified further to the west, associated with detachment systems to the south of the Mauléon basin (Jammes *et al.*, 2009; Masini *et al.*, 2014; Cadenas *et al.*, 2021). Tectonic breccias positioned along the basement-cover interface have been interpreted as tectonic contacts inherited from extension during the Cretaceous rifting. In the same line of thought, ductile-brittle shearing recognized in the pre-rift sedimentary cover is interpreted as reflecting differential stretching between cover and basement (Clerc *et al.*, 2015, 2016; Lagabrielle *et al.*, 2020), which is not entirely accommodated above the Triassic evaporites. Other top-basement shear zones in the NPZ involving mylonitized crustal lenses (granulite, quartzite) in contact with the syn-rift cover and the mantle, indicate ductile crustal shearing associated with rift-related and denudation of both the basement and mantle below the sedimentary cover (Asti *et al.*, 2019, 2021; Lagabrielle *et al.*, 2019a, 2019b, 2020). Finally, recent works in the western NPZ (*i.e.*, the Chaînons Béarnais) suggest that hydraulic fracturing of the Mesozoic cover by hydrothermal fluid circulations during the syn-rift Cretaceous extension may be a common process (Salardon *et al.*, 2017; Corre *et al.*, 2018; Incerpi *et al.*, 2020b). Fluids that form brines in the pre- to syn-rift cover are often characterized by elevated temperature and salinity. They are interpreted to result from the dissolution of Triassic evaporites (Cathelineau *et al.*, 2021; Motte *et al.*, 2021; Barré *et al.*, 2021).

3 Tectono-sedimentary evolution of the Agly Massif and breccias in the eastern North Pyrenean Zone: an overview

The Agly basement massif shapes the most eastern part of the North Pyrenean Massif. It consists of a condensed metamorphic pile characterized by increasing Variscan metamorphic conditions from chloritoschists in the north-north-east to granulites in the south-south-west (Delay, 1989; Olivier *et al.*, 2008; Tournaire Guille *et al.*, 2019; Siron *et al.*, 2020). The Saint Arnac and Ansignan granitic plutons form kilometric intrusions in low-metamorphic schists and micaschists to the North and high-grade granulites to the South, respectively (Fig. 1b). A polyphased deformation history is documented in the Agly Massif as defined by 1) an early stage of distributed and high-temperature deformation and 2) low-angle extensional mylonitic shear zones that are predominately localized in granulitic rocks and developed in retrograde conditions, that caused the metamorphic pile thinning (Delay, 1989; Bouhallier *et al.*, 1991; Althoff *et al.*, 1994; Olivier *et al.*, 2004, 2008; Vanardois *et al.*, 2020). The Variscan age of the distributed gneissic deformation (Stage 1), along with the magmatic fabric in the plutons, are largely accepted, but the age of shear zones (Stage 2) is disputed. Some authors have proposed that they developed during Variscan times (Bouhallier *et al.*, 1991; Olivier *et al.*, 2004; Vanardois *et al.*, 2020), while others have considered a strong Cretaceous imprint (Paquet and Mansy, 1991, 1992), which is also implicit in reconstructions of the Agly Massif during the Cretaceous rifting (Clerc and Lagabrielle, 2014; Clerc *et al.*, 2016). This latter hypothesis is supported by recent geochronological and thermochronological data that require (re)activation of these shear zones localized in the ductile lower part of the crust during the Aptian-Albian extension (Odlum and Stockli, 2019; Aumar *et al.*, 2022). We know that the Agly granulites represent the base of the metamorphic pile during the Late Carboniferous to Early Permian (305–295 Ma) Variscan metamorphic event, with pressures estimates between 9 and 6.6 kbar (Siron *et al.*, 2020), corresponding to a depth of 18 to 24 km. The Saint Arnac granite pluton, with an apparent thickness of 5 km, is emplaced during the same period in the Variscan upper crust, with pressure estimates comprises between ca. 1 and 3 kbar (Olivier *et al.*, 2008). Cretaceous U–Pb ages on apatite, rutile (Odlum and Stockli, 2019) and ^{40}Ar–^{39}Ar ages on biotite (Aumar *et al.*, 2022) reveal rapid cooling at 120–115 Ma in the granulite from temperatures of ca. 500 °C whereas the northern Saint Arnac pluton retains Late Carboniferous apatite U–Pb ages (Odlum and Stockli, 2019). These data implies that the Agly granulites resided in the beginning of the rifting episode between 15 and 20 km (depending on the temperature gradient considered in Aptian times), and syn-rift ductile thinning. Besides, a well-defined metasomatic event outlined by strong dequartzification and albitization of the St-Arnac and Salvezines granites is dated at 98 ± 2 Ma (early Cenomanian) by U–Th–Pb geochronology on hydrothermal monazite (Poujol *et al.*, 2010) and at 117.5 ± 0.4 Ma (middle Aptian) based on Ar–Ar dating of hydrothermal muscovite (Boulvais *et al.*, 2007). The thermal imprint of rifting is recorded in the Mesozoic cover by the southward increase of temperatures ranging from 200 °C in the Saint Paul de Fenouillet syncline to 600 °C in Boucheville syncline, which is related to gradual crustal thinning (Clerc, 2012; Chelalou, 2015; Ducoux *et al.*, 2021; Fig. 1c). In this respect, the presence of a peridotite body in contact with metamorphosed pre- and syn-rift rocks on the northern flank of the Boucheville syncline (Fig. 1b) shows that hyper-extension and exhumation of sub-continental mantle occurred to the south of the Agly Massif (Clerc *et al.*, 2016).

The folded Mesozoic cover is exposed in the Saint Paul de Fenouillet, Bas-Agly and Boucheville synclines (Figs. 1b and 1c). The base of the sedimentary cover comprises the Triassic limestones, marls and evaporites that are locally exposed along the North-Pyrenean Frontal Thrust and above the Mouthoumet and the Agly massifs (Fig. 1b). The Triassic is topped by a succession of Lower Jurassic limestones alternating with marls that are part of a wide carbonate platform that developed until the Upper Cretaceous (Peybernès, 1976, 1978a, 1978b, 1979; Jaffrezo, 1980). The Aptian period (121.4–113.2 Ma, Gale *et al.*, 2020) is marked by a brutal change of sedimentation that reflects the onset of the Cretaceous rifting. This is indicated by the deposition of alternations of discontinuous levels of silty limestones and marls, condensed succession, hardgrounds and the local presence of paleokarsts and bauxite deposits on the northern flank of the Saint Paul de Fenouillet syncline and in the western extremity of the Bas Agly syncline (Esquevin *et al.*, 1971; Combes, 1990; Fig. 1b). The transition from the latest Aptian to the earliest Albian depicts the onset of increased subsidence that is recorded by the deposition of black flyschs until the early Cenomanian (Berger *et al.*, 1993; Ford and Vergés, 2021). It has also been suggested that the syn-rift sedimentation in the Cretaceous was strongly controlled by the Triassic salt mobility. This is supported by the interpretation of several salt-walls structures aligned above major high-angle basement normal faults. These passive diapiric structures individualize syn-rift mini-basins in the decoupled Mesozoic cover; each marked by strong variation of the thickness of sediments interpreted as halokinetic sequences. Finally, the transition from syn- to post-rift basin evolution is indicated by a gradual evolution of the depositional environment towards shallower carbonate platform facies during the upper Cenomanian (Berger *et al.*, 1997). The European side of the Pyrenean rift was then inverted in the upper Cretaceous, which ultimately resulted during the Eocene in moderate thick-skinned shortening (about 6 km) in Agly Massif (*e.g.*, Ternois *et al.*, 2019; Al Reda *et al.*, 2021). Most authors involve only limited decoupling of the Mesozoic over relative the parautochthonous basement during the Cenozoic (*e.g.*, Ternois *et al.*, 2019; Ford and Vergés, 2021; for the most recent). A recent study has suggested however that the Mesozoic cover might have been displaced significantly northward on top of the Agly Massif (Ducoux *et al.*, 2021). This is partly based on the high RSCM temperatures above 500 °C measured in the Bas Agly in the north relative to temperature in the Agly Paleozoic basement in the south. But these temperatures could alternatively reflect crustal thinning to the North of the Agly Massif (*e.g.*, Clerc and Lagabrielle, 2014). The region was then covered by up to 1–1.5 km-thick post-orogenic deposits from 30 Ma (Ternois *et al.*, 2019; Al Reda *et al.*, 2021), which were then partially eroded during the last 10 Myrs (Fillon *et al.*, 2021).

Because the Mesozoic cover recorded the succession of rifting, tectonic inversion, salt tectonics and fluid flow events, it is not surprising that the origin of the breccias has been diversely interpreted (Fig. 2). The presence of Albian clasts, as documented in the first description of the breccias, led to interpret of the breccias as polygenic post-metamorphic and therefore post-rift (post Cretaceous) deposits (Mattauer and Proust, 1962). This hypothesis was later supported by more detailed mapping of these breccias suggesting they are deposits unconformably overlying both basement and cover, and therefore syn- to post-orogenic deposits (Berger *et al.*, 1993). Later descriptions suggested that breccia systems with similar characteristics are in fact interstratified with hemipelagites containing Paleocene planktonic foraminifera within their matrix (Peybernès *et al.*, 2001a). This so-called "Danian revolution" theory was later rejected based on sedimentological, magmatic, and geodynamic counterarguments (Canérot, 2006; Bilotte *et al.*, 2007) and could alternatively be of tectonic, diapiric or tectono-karstic origin. Two contradictory hypotheses have been proposed. On the one hand, breccias are syn-rift sedimentary deposits related the Cretaceous rifting (Clerc, 2012; Chelalou, 2015; Kernif *et al.*, 2020, 2021) or tectonic structures formed at the base of the decoupled Mesozoic cover (Clerc *et al.*, 2016). Pre-orogenic late Jurassic to mid late Cretaceous ages are corroborated by scarce *in situ* U–Pb dating of the calcite into the matrix of breccias in the Bas-Agly breccias (Kernif *et al.*, 2020). On the other hand, it is implicitly considered based on an assumed temperature gap between the cover and basement that these breccias are Cenozoic tectonic breccias (Ducoux *et al.*, 2021). These uncertainties reveal that a more detailed and specific studies on the brecciation is required before linking them to a given tectonic process.

4 Data and approach

The term breccia refers to rocks composed of angular fragments (clasts) bonded together by a particulate (matrix) or crystalline (cement) material. Several attempts have already been made in the literature, notably through the elaboration of descriptive classifications (Morrow, 1982; Laznicka, 1989; Woodcock and Mort, 2008), or by seeking to identify petrographic features of certain processes (Blount and Moore, 1969; Shukla and Sharma, 2018). But the processes of brecciations might be hardly decipherable when only looking to these first-order descriptive characteristics. Here, we rely on specific morpho- or geometrical criteria to identify the genetic processes as follows:

- the breccia texture (*i.e.*, whether the breccia is clast- or matrix-supported; the clasts being counted when superior to 2 mm in diameter as defined by Bates and Jackson (1980), its fabric (*i.e.*, whether the containing elements are organized or not), and the nature and granulometry of the matrix that can reveal the sedimentary transport, cataclastic deformation, hydraulic fracturation or salt activity;
- the diversity of clasts (*i.e.*, mono-, oligo- or poly-mictic) provides information on the source of the brecciated material;

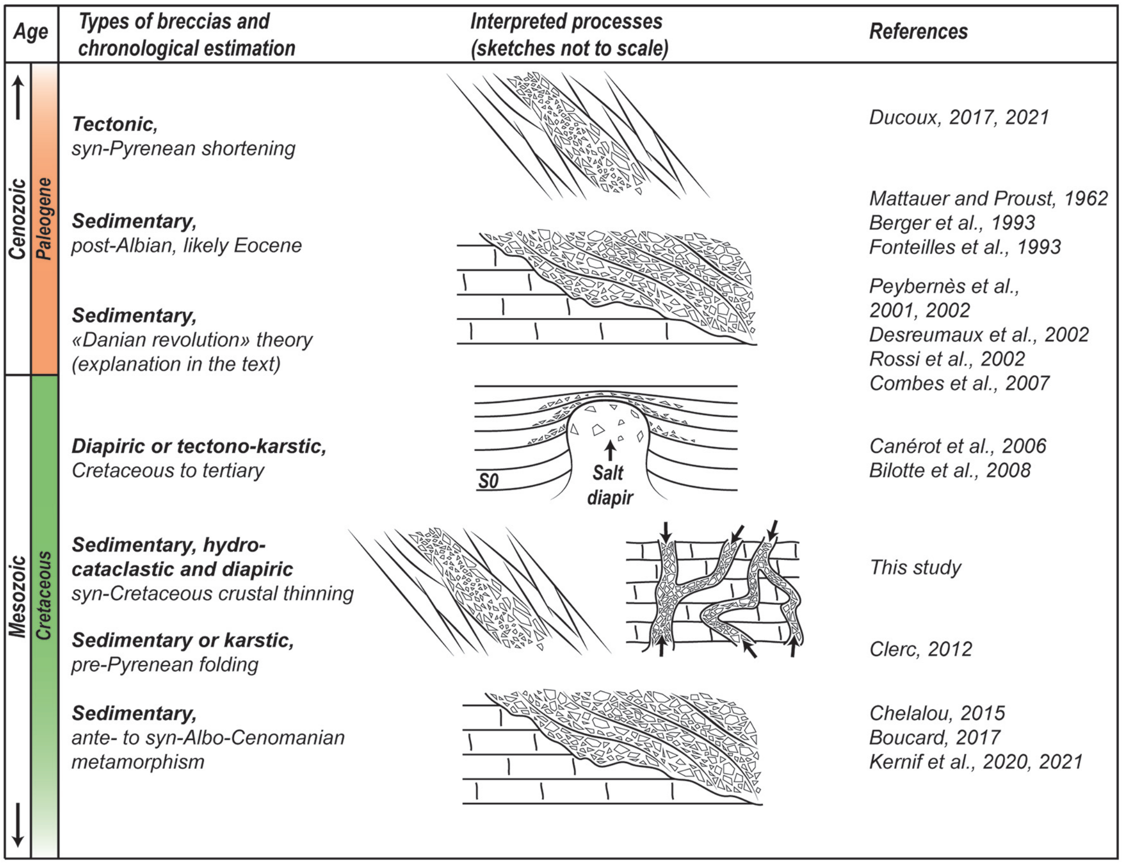

Fig. 2. Synthesis of the various hypotheses proposed in the literature for the age and processes of formation of the eastern NPZ breccias.
Fig. 2. *Synthèse des différentes hypothèses proposées concernant l'âge et les processus de formation des brèches de la Zone Nord-Pyrénéenne orientale.*

- the median and the standard deviation of the clasts size from which the sorting and the skewness are calculated (Folk and Ward, 1957);
- the roundness of clasts (Powers, 1953) and sphericity (Krumbein and Sloss, 1964) indicate the degree of maturity of the breccia providing information on transport dynamics or amount of cataclastic or fluid-assisted deformation;
- the degree of metamorphism and deformation of the clasts on the one hand, and of the whole breccia on the other hand, inform about the thermal and tectonic conditions before and after the brecciation processes.

These criteria have been applied on the different breccias of the Agly area either in the field or on sample photographs completed by thin-sections. Because the interpretation of breccias first requires identifying the stratigraphic age of the reworked material, one of the essential prerequisites is the precise knowledge of the regional stratigraphy. Based on existing regional mapping and stratigraphy (Bessière *et al.*, 1989; Berger *et al.*, 1993, 1997) and our own field investigation, we have established a synthetic log in which the different facies of the Mesozoic sedimentary rocks are reported (Fig. 3). Lithology, color, and paleontological contents have allowed the identification of 5 main facies (Fig. 3):

- yellow limestones, observed in the Triassic and sporadically in the Early Jurassic;
- red-colored clays and red limestones of the Triassic or upper Early Jurassic;
- dark to black marly to silty rocks, which correspond to the Albian syn-rift formation (black), or to the upper Early Jurassic (dark grey);
- massive white limestones, which occupy the great majority of the Middle Jurassic to the early Berriasian series (often bioclastic), but which one can also be found in the Early Jurassic (rarely bioclastic);
- blue to grey limestones, which correspond to the Valanginian to late Aptian series (*i.e.*, the bioclastic urgonian facies), but which can also be found in the Early Jurassic (rarely bioclastic).

Some facies can be attributed to stratigraphic levels (*e.g.*, the blue to grey limestones) based on the metamorphic nature of source rocks in the region, which often removes the bioclastic content and homogenizes their crystalline structure. The identification of pre-Triassic material present in breccias is

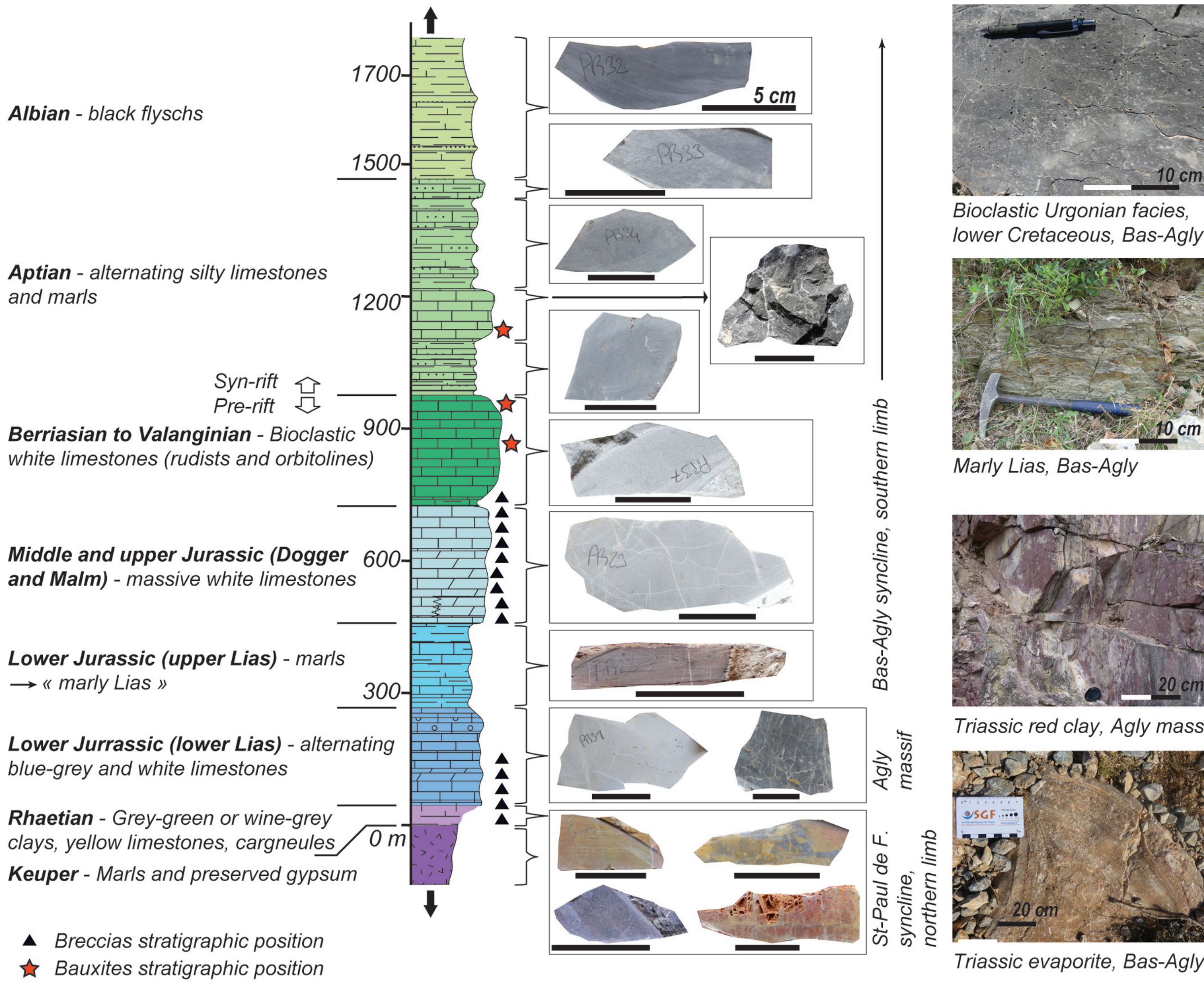

Fig. 3. Synthetic lithostratigraphic log, samples and field photographs of the Mesozoic cover from the Agly region established after Bessière et al. (1989), Berger et al. (1993, 1997), and our own field mapping. Black triangles and red stars represent the stratigraphic position of breccias and bauxites observed in the field, respectively. Abbreviation: St-Paul de F.: Saint-Paul-de-Fenouillet syncline.

Fig. 3. *Log lithostratigraphique synthétique et illustrations des principaux faciès de couverture dans la Zone Nord-Pyrénéenne orientale d'après Bessière* et al. *(1989), Berger* et al. *(1993, 1997) et notre propre travail cartographique. Abréviation : St-Paul de F. : Synclinal de Saint-Paul-de-Fenouillet.*

based on our petro-structural mapping of the Agly Massif and the abundant literature (Delay, 1989; Berger *et al.*, 1993; Tournaire Guille *et al.*, 2019; Siron *et al.*, 2020).

These criteria once converted into categorical data were used to perform quantitative analyses with PAST 4.2 software (Hammer *et al.*, 2001) to 1) ensure the statistical significance of the different types of breccias recognized in the field and 2) to explain similarities and dissimilarities between them. An Agglomerative Hierarchical Clustering (Rokach and Maimon, 2005) using Euclidean distance computed with an UPGMA algorithm (AHC) was used to determine cluster of similar samples. A Principal Coordinates Analysis (PCOa) performed with the Gower distance (Gower, 1966) allowed the visualization of the distribution of breccia samples in a petrographical space and the exploration of descriptive characteristics uniting the clusters. The robustness of the resulting clusters has been assessed using a one-way pairwise analysis of similarities (ANOSIM) test (Clarke, 1993).

5 Results

Breccias are exposed in the lower part of the Mesozoic cover on both flanks of the Bas Agly and Boucheville syncline, as well as in the center of the Agly basement massif where they follow two N110°E-trending structural lineaments (Fig. 1b). At the scale of the eastern NPZ, they are mainly localized in the Metamorphic Zone, and near the contact zones between the cover and the basement (Figs. 1b and 1c).

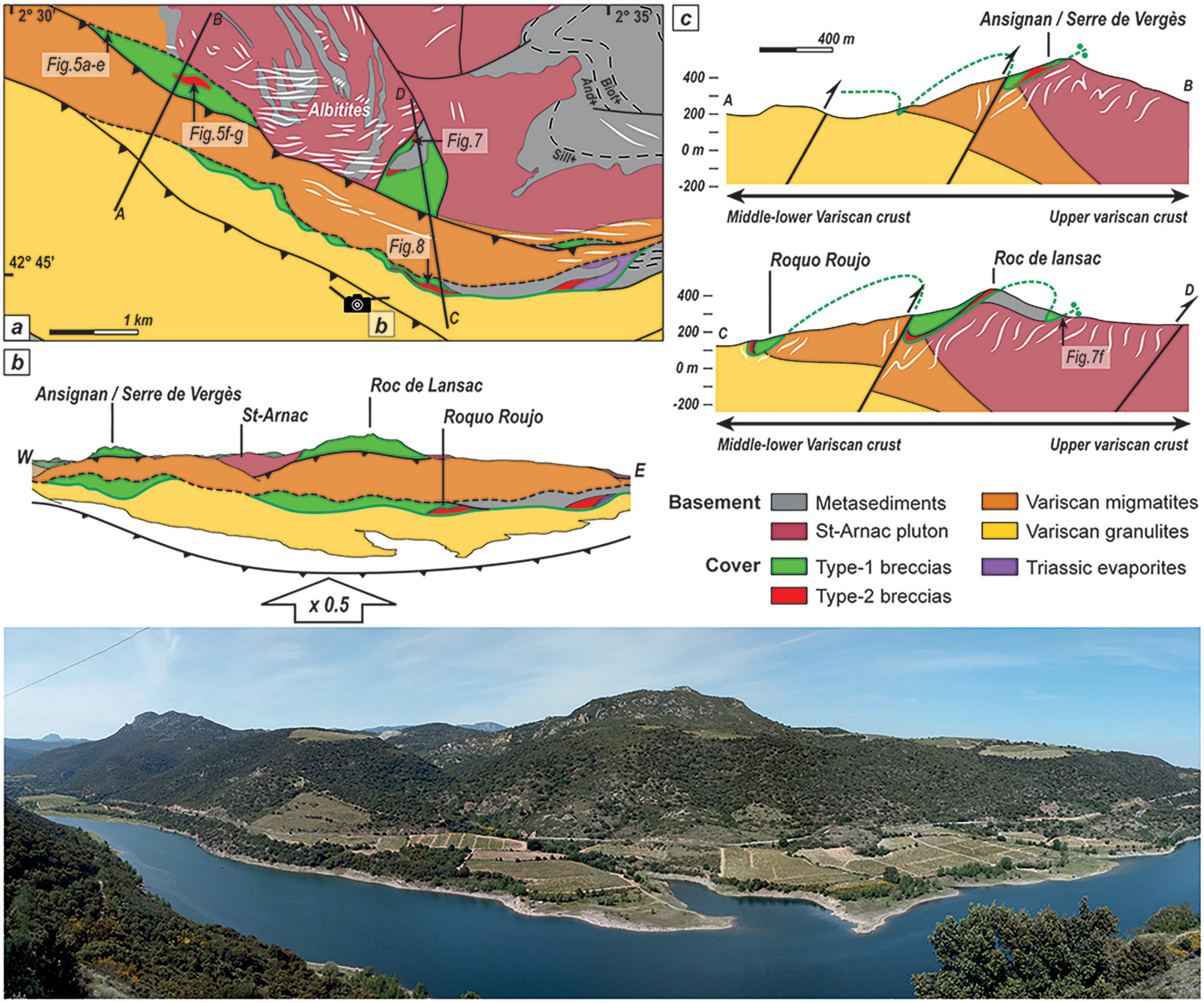

Fig. 4. Structural map (a), panorama (b) and cross-sections (c) of the breccias studied in the Agly Massif. Location in Figure 1b.
Fig. 4. *Carte structurale (a), panorama (b) et coupes sériées (c) au centre du massif de l'Agly. La localisation et la légende sont sur la Figure 1b.*

5.1 Type-1 and type-2 breccias in the centre of the Agly Massif

In the centre of the Agly Massif the breccias that composed the Mesozoic cover reach a maximum thickness of around 100 m and form high topographic ridges that contrast with open valley and smooth relief of the weathered basement rocks (Fig. 4). In detail two N110°E-oriented ridges can be distinguished: i) the Ansignan/Serres de Vergès and Roc de Lansac to the North, and ii) the Roquo Roujo to the south.

5.1.1 Ansignan/Serre de Vergès breccia

The Ansignan/Serre de Vergès breccia (Figs. 4a and 4b) is separated from the basement rocks by two subvertical fault zones showing hydrothermal alteration of basement rocks in the form of albitization and hematization. The first type of breccias, defined in this study as type-1 breccia, is recognized regionally and named the "Ansignan facies" (Fig. 5a). It consists of a polymictic agglomerate of whitish/greyish marble in a carbonate-rich red clayey to sandy matrix. The clasts are sub-angular to well-rounded, and moderately sorted at a first order, with sizes ranging between 2 mm and 10 cm. Some isolated blocks however can reach several tens of centimetres. When compared to the type of possible source rocks (Fig. 3) we infer that the clasts pertain to Triassic to Aptian series with no younger clasts involved (Fig. 5b). At the contacts with the basement, clasts originating from the cover are associated with a minor fraction (max. 5%) of schists, hematite, quartz or felsic fragments. This is especially visible in the western part of the Serre de Vergès (Figs. 4a, 5c and 5d). These basement-type elements are sourced from the upper Variscan metamorphic pile, *i.e.*, the St-Arnac pluton and its Paleozoic hosting-rocks. The quartz-schist association reveals the reworking of the

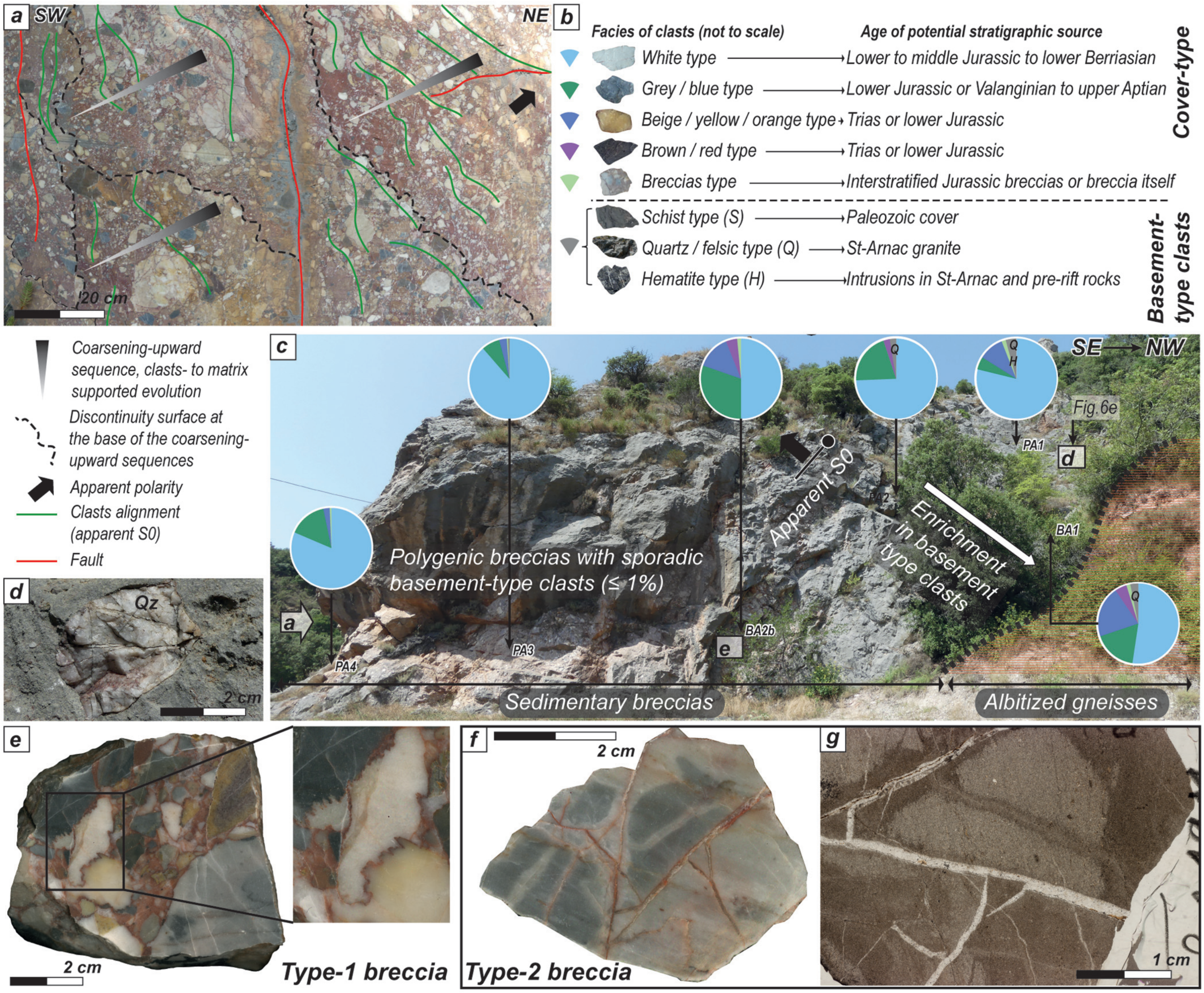

Fig. 5. Field photographs and polished sections of the Ansignan/Serre de Vergès breccia (see Fig. 4a for location). A) Interpretation of type-1 breccia showing sedimentary figures. B) Categories and stratigraphy of source rocks for the different clasts labeled as colored symbols. C) Panorama showing type-1 breccia in contact with the basement rocks. Colored pie charts that represent the proportion of clasts of studied samples based on B). D) Pluri-centimetric clast of quartz in carbonate matrix near the contact with the basement. E) Sample of type-1 breccia highlighting the marble aspect with static recrystallization of both matrix and clasts and stylolites. F) and G) Sample and thin section of type-2 breccias characterized by angular clasts and calcite veins.

Fig. 5. *Illustrations des brèches d'Ansignan et de la Serre de Vergès (voir la localisation sur la Fig. 4a). A) Interprétation des brèches de type-1 montrant les figures sédimentaires. B) Répartition stratigraphique des strates sources des clastes. C) Panorama montrant les brèches de type-1 en contact avec le socle. Les diagrammes circulaires montrent les proportions de clastes dans les échantillons étudiés. D) Claste de quartz pluricentimétrique au sein de la matrice carbonatée au contact avec le socle. E) Echantillon de brèche de type-1 montrant un aspect marmorisé avec une recristallisation statique de la matrice et des clastes et des joints stylolitiques. F) et G) Échantillons et Lame Mince de brèches de type-2 caractérisés par des clastes angulaires et des veines calcitiques.*

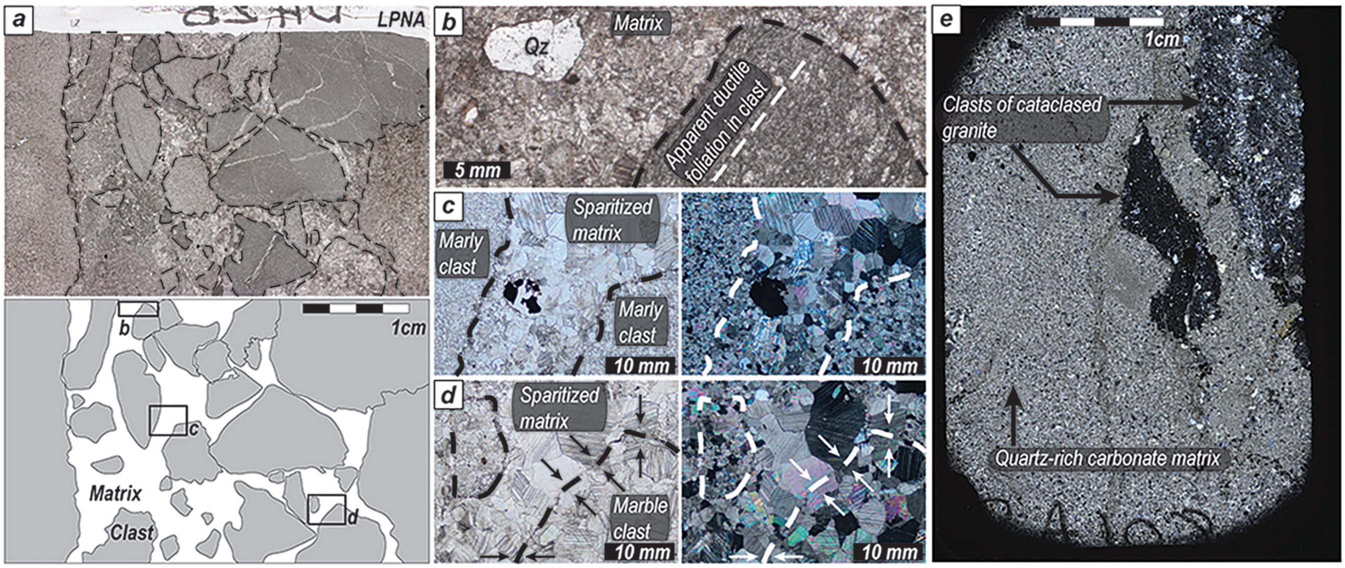

Fig. 6. Thin section of type-1 breccias in the Serre de Vergès. A) Facies enriched in Mesozoic marble clasts (collected away from the contact with the basement) with zooms showing small clasts of quartz into the matrix and foliation in marble clasts (B), sparitic matrix (C) and static recrystallization of the clasts/matrix interfaces (D). E) Facies enriched in basement clasts (collected at the vicinity of the contact with the basement; see location in Figure 5c.

Fig. 6. *Microphotographies des brèches de type 1 de la Serre de Vergès (voir la localisation sur la Fig. 4a). A) et B) Faciès enrichi en clastes marmorisés mésozoïques et des grains de quartz dans la matrice carbonatée (B). C) Zoom sur la matrice recristallisée en sparite. D) Zoom sur l'interface claste/matrice montrant une recristallisation statique. E) Faciès enrichi en microclastes de socle (localisation de l'échantillon sur la Fig. 5c).*

sillimanite-bearing micaschists level, which contains numerous quartz veins in the area. Quartz grains are also present in a significant proportion in the matrix, in the form of silty to sandy grains visible in thin sections (Figs. 6a and 6b). At distance from the contact with the basement, the type-1 breccia (Ansignan) depicts changes in matrix colors and sometimes a coarsening-upward distribution of clasts that outline stratigraphic sequences (Fig. 5a).

The clasts of sedimentary cover retrieved in the type-1 breccia show large sparitic grains and diffuse edges of the allochems of marbles that reveal recrystallization. The matrix appears less recrystallized than the clasts although both the aspect in the field and the local sparitization of the matrix suggest recrystallization (Fig. 6c). The static recrystallization indeed is particularly striking in thin sections, as argued by the removal of clasts/matrix boundaries (Fig. 6d). Pressure-solution processes during burial and/or tectonics are indicated by stylolites in clasts/clasts or clasts/matrix boundaries (Fig. 5e). Clasts from the St-Arnac granite that are recognized in breccia overlying the granite show cataclastic deformation (Fig. 6e).

A second breccia, called type-2, is exposed in the central part of the Serre de Vergès. It is a clast-supported breccia that consists of a mono- to oligomictic association of white and blue marble clasts and lack of elements from the basement (Fig. 5f). The clasts are sub-angular to angular, with a very low degree of sphericity. Clasts are interpreted as originating from the Liasic series, strongly metamorphosed and foliated. In contrast to type-1 facies, type-2 breccias are characterized by fluid-assisted fractures as outlined by the numerous calcite veins and cement (Fig. 5g).

5.1.2 Roc de Lansac breccias

Breccias exposed in the Roc de Lansac are found in tectonic contact with St-Arnac granodiorite in the hangingwall of a fault zone marked by moderate- to low-angle dip, an apparently normal sense of shear and an albitite-rich fault-core (Figs. 4, 7a and 7b). Both type-1 and type-2 breccias previously described are found juxtaposed. Near the contact with the fault, a polymictic breccia typical of type-1 is documented in which the size of marble clasts can locally exceed one meter in diameter (Fig. 7c). The stratigraphic ages of identified source rocks range from Triassic to Aptian. The proportion of basement clasts increases to more than 75% near the contacts with the basement, a notably higher proportion than for Ansignan/Serre de Vergès (Fig. 7d). They are essentially schists and quartzites or quartz pebbles (Fig. 7e) embedded in the typical red, finely particulate carbonate-rich matrix, which occupies up to 75% of the mass of the breccia (Fig. 7f). Clasts of type-1 breccia show the same metamorphic imprint and evidence for ductile deformation as in the Ansignan/Serre de Vergès breccias. The matrix is also often recrystallized. This type of breccia is characterized by a high concentration of white calcite cement and veins at both outcrop and individual clast scales (Fig. 7d). Because the density of white calcite cements can reach more than 50% of the breccia mass, this fluid-assisted highly fractured breccia is considered

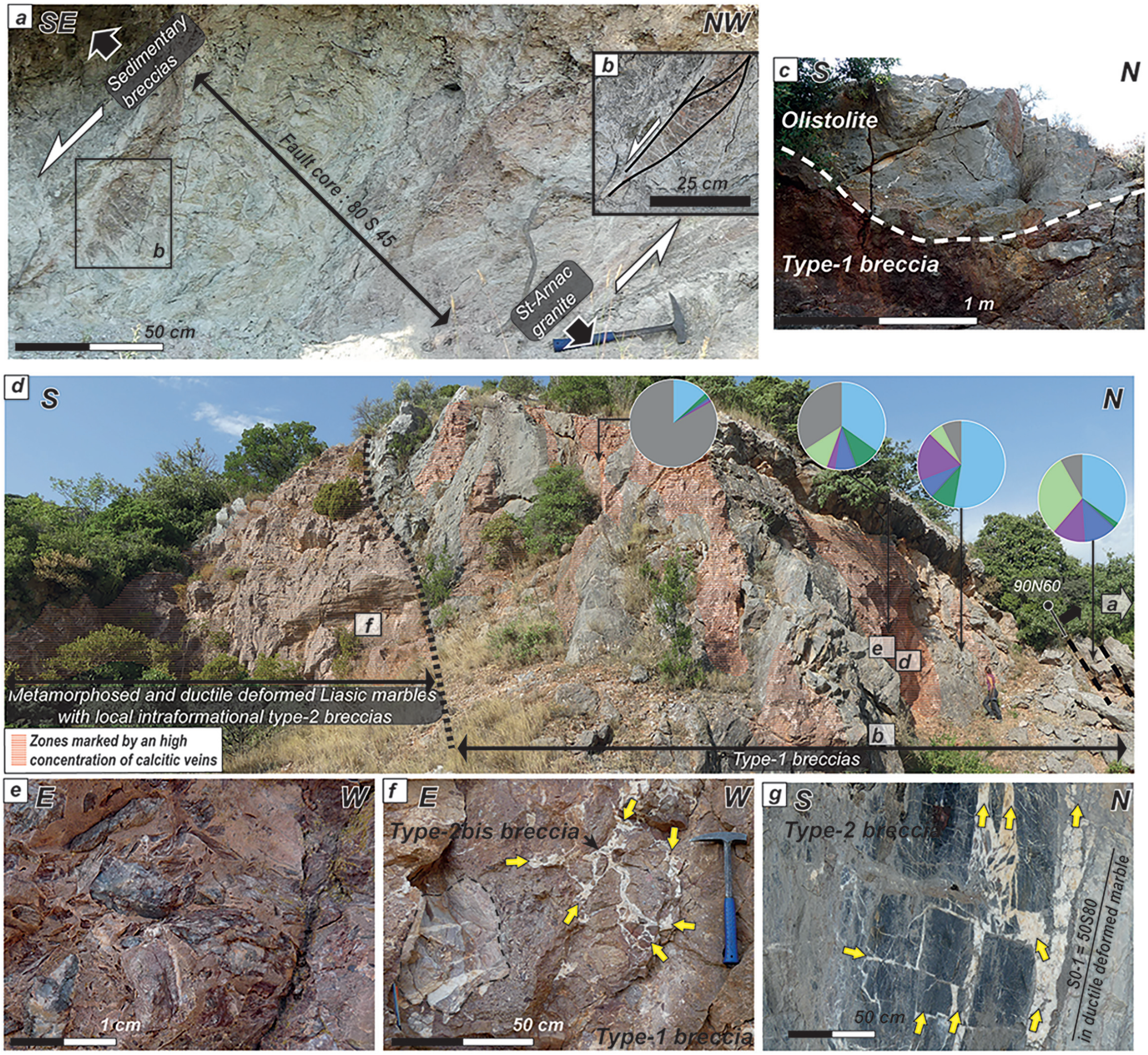

Fig. 7. Field photographs of the Roc de Lansac breccias (see location in Fig. 4a). A) and B) Fault zone at the contact between the St-Arnac granite, an upper albite alteration front (footwall) and the type-1 breccias (hangingwall). C) Jurassic marble block. D) Panorama showing the juxtaposition of type-1 breccias with the Early Jurassic marbles that contain type-2 breccias. The pie charts represent the proportion of clasts categorized of the studied samples. E) Clasts of quartz and schists from the Variscan basement. F) Calcite cements and veins in type-1 breccias (locally type-2bis when the amount of veins is > 50%). G) Type-2 breccias showing long and angular parallel clasts supported by white calcite cement and veins orthogonal to S_{0-1}.

Fig. 7. *Illustrations des brèches du Roc de Lansac (voir la localisation sur la Fig. 4a). A) et B) Zone de faille au contact entre le pluton granitique de St-Arnac montrant un front d'altération et les brèches de type-1.C) Bloc de marbre jurassique interprété comme un olisthболее au sein de la brèche de type-1. D) Panorama montrant la juxtaposition des brèches de type-1 avec les marbres jurassiques inférieur contenant les brèches de type-2. Les diagrammes circulaires montrent la diversité proportionnelle des clastes (légende en Fig. 5b). E) Clastes de quartz et schistes paléozoïques dans la brèche de type-1. F) Brèche de type-1 passant localement à une brèche de type-2bis lorsque le liant est calcitique. G) Brèche de type-2 montrant des clastes rectangulaires parallèles cimentés par de la calcite et des veines orthogonales à la* S_{0-1}.

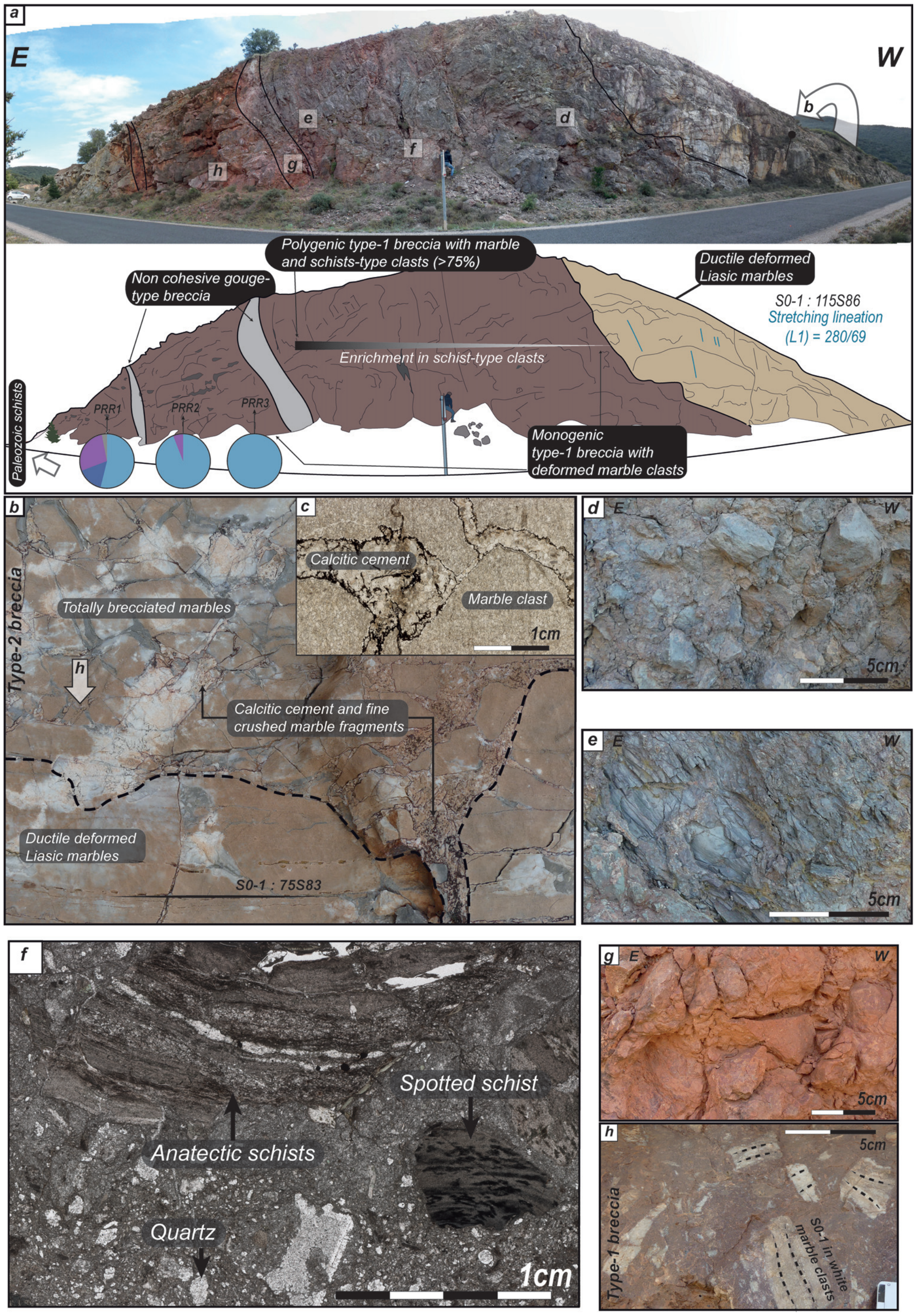

Fig. 8. A) Roquo Roujo site (location in Fig. 4a) showing structural relationships between Lower Jurassic marbles and type-1 breccias. Pie charts represent the proportion of clasts (see Fig. 5b for captions). B) and C) Type-2 breccia found near the base of the Agly Mesozoic cover. D) Type-1 breccia enriched in Lower Jurassic marble clasts. E) Type-1 breccia enriched in schist clasts. F) Thin section of the type-1 breccias highlighting the high concentration of quartz grain in the matrix and of various Paleozoic schists. G) Non-cohesive gouge type-breccia. H) Matrix supported type-1 breccia showing the foliation in white marble clasts.

Fig. 8. *Illustrations des brèches de Roquo Roujo (voir la localisation sur la Fig. 4a). A) Panorama et « line-drawing » montrant les relations structurales entre les marbres du Jurassique inférieur et les brèches de type-1. Les diagrammes circulaires montrent les différentes proportions de clastes (légende en Fig. 5b). B) Gouge de faille non cohésive. C) Brèche de type-1 enrichie en clastes de schistes paléozoïques. D) Brèche de type-1 enrichie en clastes de marbres du Jurassique inférieur. E) Brèche de type-1 à dominance de matrice montrant la foliation dans les clastes de marbres. F) Lame mince d'une brèche de type-1 montrant la forte concentration de grains de quartz dans la matrice et l'abondance des clastes de schistes paléozoïques. G et H) Brèche de type-2 collectée près de la base de la couverture mésozoïque de l'Agly montrant les ciments calcitiques et la déformation ductile des marbres.*

distinct from type-1 breccias and named type-2bis (Fig. 7f). A few 30 m to the south of the low angle normal fault, type-1 breccias lie in contact with the deformed Lower Jurassic marbles (Fig. 7d) through a transitional domain represented by type-2 breccia made of Early Jurassic clasts similar to the Ansignan/Serre de Verges system (Fig. 7g). The calcite cement that supports the foliated clasts is parallel to S_{0-1} while veins are perpendicular.

5.1.3 Roquo Roujo breccias

The Roquo Roujo breccias are exposed at the interface between Variscan migmatites and granulitic rocks, one kilometre to the south of the Roc de Lansac (Fig. 4). The base of the Roquo Roujo breccia system is observed to the East of the outcrop shown in Figure 8a. There, Early Jurassic marbles bear a well-defined stretching and mineral lineation marked by the alignment of scapolite minerals. These marbles are characterized downwards by intraformational type-2 breccia, composed of monomict clasts made of foliated Early Jurassic marbles (Figs. 8b and 8c). To the East, the first type of breccia contains elements of Early Jurassic marbles and Palaeozoic schists. Near the contact with the marbles, clasts are mainly composed of foliated marbles supported by a silty to sandy carbonate-rich matrix (Figs. 8a and 8d). Moving structurally downwards (eastwards), the clasts set is enriched in schist elements (Figs. 8a and 8e). In thin section, these clasts correspond to spotted-schists and micaschists with quartz veins (Fig. 8f), suggesting they originated from the Palaeozoic cover. Further East, the breccia is intersected by a zone of non-cohesive breccia of about 1.5 m thick (Figs. 8a and 8g), composed of red sandstone clasts. They are rolled, locally jointed but mainly supported by a silty to sandy matrix of mixed carbonate and quartz grains. In the easternmost part of the outcrop, type-1 breccia is exposed (Fig. 8h) containing strongly metamorphosed and foliated white marbles, similar to the Early Jurassic succession.

5.2 Type-3 and type-4 breccias in the Bas-Agly and Boucheville synclines

5.2.1 Belesta breccia: Eastern Boucheville syncline

At the periclinal termination of the Boucheville syncline, a few hundred metres East of the village of Belesta, two outcrops allowed us to examine the structural relationships between Cretaceous deposits of the Boucheville syncline and the basement (Fig. 9). In the first outcrop, EW-oriented and moderately south-dipping low-grade mylonitic shear zones are observed in the basement (Figs. 9a and 9b). Laterally southward, the mylonites show a transition to a brittle fault core marked by dip-slip movements on shears fractures parallel to the ductile shear planes (Figs. 9a and 9b). The hangingwall of this ductile-brittle shear zone is represented by a 250-m thick brecciated zone that involves both cover and basement materials. This type-3 breccia contains clasts of Jurassic to Aptian marbles, Paleozoic schists, anatectic rocks, and mylonitic granulites. There is a clear southward enrichment of cover clasts away from the fault core (Fig. 9a). The clasts are supported and cemented by silty to sandy elements made from the clasts themselves. The whole mélange has a washed-out appearance due to the high concentration of calcite cement (Fig. 9c). A few hundred meters to the west, the mélange zone is affected by asymmetric pseudo-boudinage defining an extensional shear zone (Fig. 9d).

5.2.2 Bas-Agly breccia: southern limb of the Bas-Agly syncline

The southern flank of the Bas-Agly syncline is represented by two kilometer-scale inclined folds verging to the North (Fig. 10).

Near the village of Calce, the lowermost Lower Jurassic deposits are marked by widespread ductile deformation and an intense brecciation. Ductile deformation is attested by well-developed flat-lying foliation parallel to the stratification plane (S_{0-1} structures) bearing N-NE plunging stretching lineations and several occurrences of boudinage of limestone level (Figs. 10 and 11a). To the North-West of Calce, boudins are interrupted by numerous small-scale high angle normal faults (Figs. 11b and 11c). These shear fractures are associated with calcite veins perpendicular to S_{0-1} (Fig. 11d). Where the intensity of brittle tectonics increases the ductile fabric is disorganized, and the boudinaged structures are replaced by type-2 breccias (Fig. 11b) made of heterometric (from 2 mm to more than 10 cm) clasts of foliated Early Jurassic marbles, involving a small proportion of gypsum. Evaporites are also observed sporadically in the form of small circumvolution below the boudins of marbles. To the West, in the Col del Loup area (Fig. 10), the same type-2 breccia is observed at the interface between the sheared Paleozoic schists and the ductile deformed Mesozoic basal cover.

In the Col de la Dona (Figs. 10a and 10c), the basement/cover interface shaped by the contact between the Ordovician-Silurian schists and the Early Jurassic marbles (including type-2 breccia) is outlined by a distinct type of breccia. The thickness of this type-4 breccia level is about 5 m. It consists of a polymictic association of angular and sub-spheric clasts exclusively made of Triassic, Lower Jurassic and Ordovician-Silurian lithologies (Fig. 11e) supported by a recrystallized calcarenitic matrix.

Another category of breccias referred to as type-5 and type-5bis breccias are found in Lower Jurassic at the vicinity of the transition with the Early Cretaceous limestones of the Bas-Agly syncline (Fig. 10). The core of type-5 breccias corresponds to massive tens to hundreds of meters thick oligomictic to polymictic poorly sorted agglomerate made of metamorphosed limestones and marls, white and blue, often foliated, sub-angular and with a low degree of sphericity (Fig. 11f) with bedding surface occasionally preserved. The latter are discontinuous but the overall anticline structure can be recognized (Fig. 10c). The majority of the clasts are sourced from the Middle Jurassic to the Lower Cretaceous stratigraphic levels with subordinate beige/yellow and brown/red Early Jurassic and Triassic carbonates (Fig. 11f). Breccias are progressively enriched upsection in dark clasts of silty limestones, typical of the Aptian-Albian series (Fig. 11f). No clasts from the basement were recognized in this type-5 facies. This matrix can be associated or replaced by a more or less high concentration of calcite veins (Fig. 11g). Some occurrences of gypsum are found exposed at the base of the

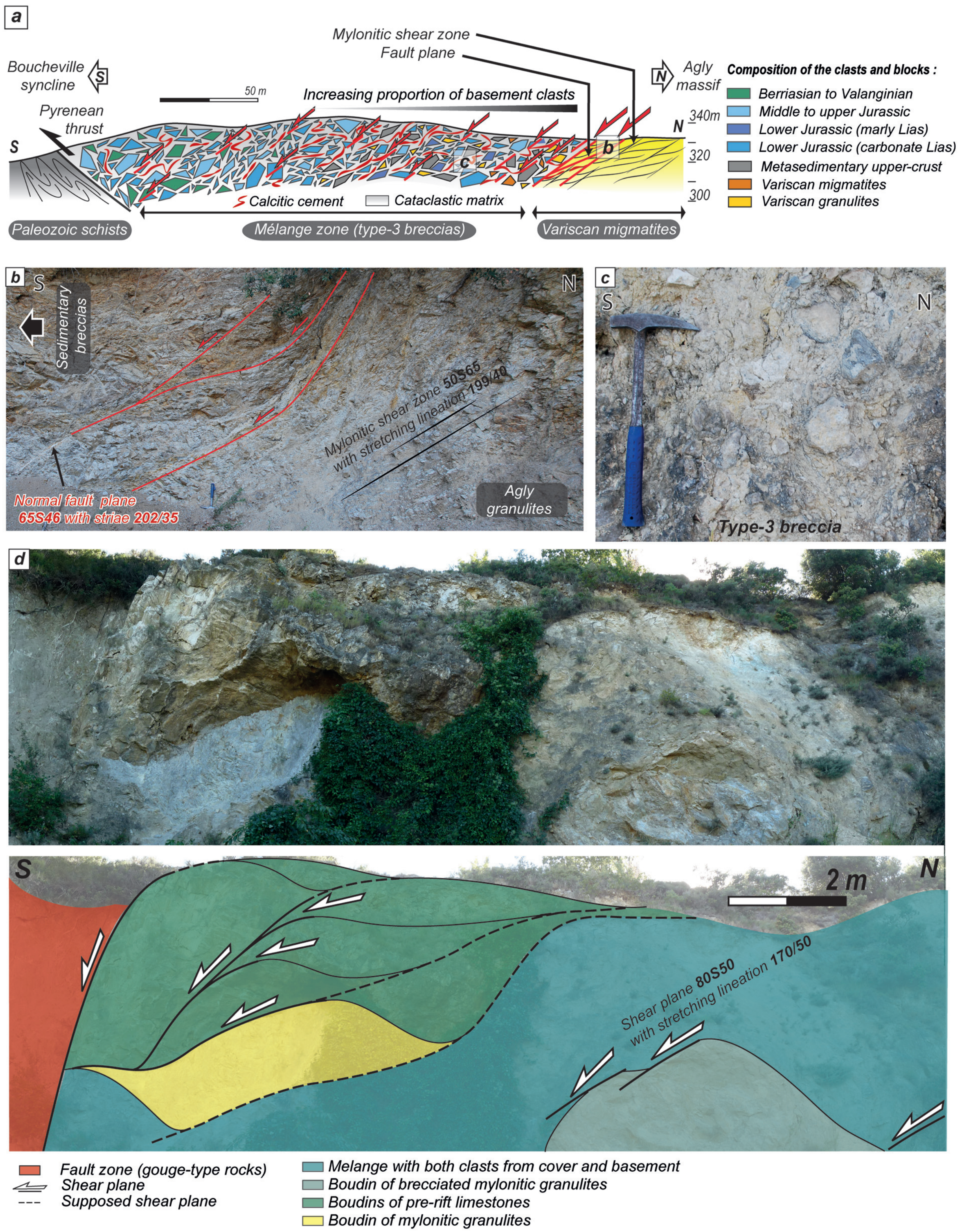

Fig. 9. A) Schematic cross-section of the mélange zone in the vicinity of Belesta, at the interface between the Agly basement and the Mesozoic cover in the Boucheville syncline. B) Photograph of the granulitic mylonites at the contact. C) Photograph of the type-3 breccia. D) Panorama and interpretation of the deformed mélange zone. Location in Figure 1b.

Fig. 9. *A) Coupe schématique de la zone de mélange à proximité de la localité de Belesta. B) Photographie d'une brèche de type-3. C) Photographie et schéma interprétatif de la zone de mélange à l'est de Belesta.*

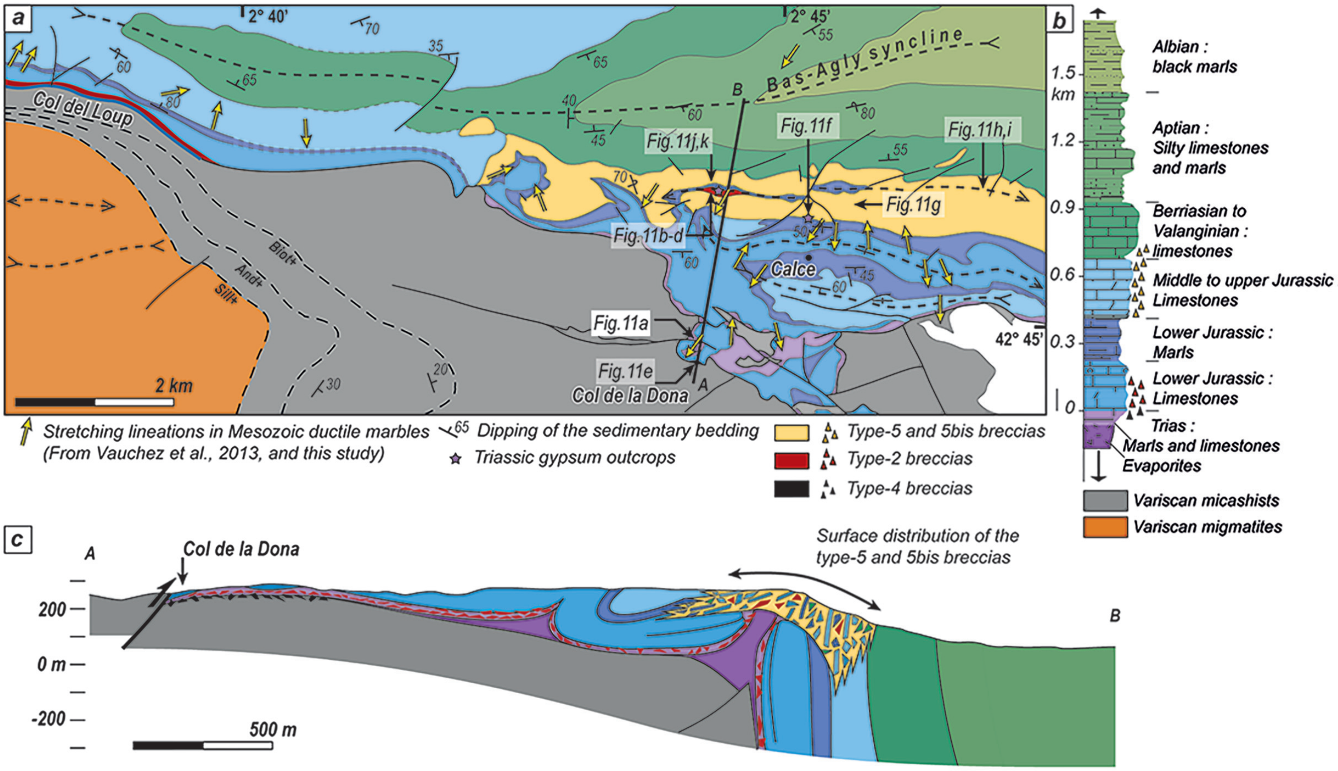

Fig. 10. A) Detailed geological map of the southern part of the Bas-Agly syncline (Location in Fig. 1b). B) Lithostratigraphic log of the Mesozoic cover showing the structural position of the different types of breccias. C) N-S cross-section of the southern Bas-Agly.
Fig. 10. *A) Carte structurale détaillée du synclinal du Bas-Agly. B) Log lithostratigraphique de la couverture Mésozoïque du Bas-Agly. C) Coupe orientée NS de la partie sud du Bas-Agly.*

breccias (Fig. 11h), but also within type-5 as convolution among breccia such as observed at the base of the Middle Jurassic or directly as a constituent of the matrix (Figs. 11g and 11i). Toward the axis of the anticline, a large number of vertical pipes, oriented between N0° and N45°E, filled with a mix of gypsum and carbonate mud (Fig. 11g).

Some specific breccias, called here type-5bis, are found associated with some specific stratigraphic interfaces in the form of metric to plurimetric level, parallel to the stratification (Figs. 11j and 11k). They can be well identified in the field at the transition between the lower Upper Jurassic blue/grey banded limestones and the Kimmeridgian white massive limestones. The clasts are mono- to oligomictic, heterometric (2 mm to tens of centimeters), angular and relatively tabular, and often parallel to the stratification and supported by red carbonate-rich mud. The upper and lower border of these interstratified systems are marked by the dissolution of marbles and the mud infiltration into fractures (Fig. 11j).

5.3 Testing the robustness of breccia type identification: a statistical approach

Field investigations helped to distinguish seven different types of breccias (*i.e.*, types 1, 2bis, 2, 3, 4, 5 and 5bis), based on sedimentological, structural, and petrographical characteristics. In this paragraph, our objective is to provide a quantitative validation of the separation between breccias we made in the field using a qualitative approach. We hypothesize that some of the different types may be genetically linked.

The significance of the seven field-base types is tested by performing an Agglomerative Hierarchical Analysis (AHC) based on the main sedimentological and petrographical characteristics (see part III for methodological details). The Principal Coordinates Analysis (PCOa), based on the same dataset, is used to reveal petrographical similarities between the clusters identified by the AHC. A set of 57 samples has been collected to reflect the variability of breccias at the outcrop scale from which the petrographical descriptors have been categorized into 8 characters (clast diversity and origin, breccia fabrics, lithology and granulometry of the matrix, clasts sphericity, roundness degrees and sorting) from the characteristics summarized in the Table 1.

The AHC approach returns two main clusters (Fig. 12a): the first cluster includes the group type-3 and type-4, and the group type-2 and type-2bis; the second includes the type-5bis breccia and two related sub-clusters composed of the type-1 and type-5 breccias.

The clustering results are confirmed by the distribution of the samples in the petrographic space (Fig. 12b). The first cluster (type-3, type-4, type-2 and type-2bis) is dominated by breccias with cemented clasts. The group including type-2 and

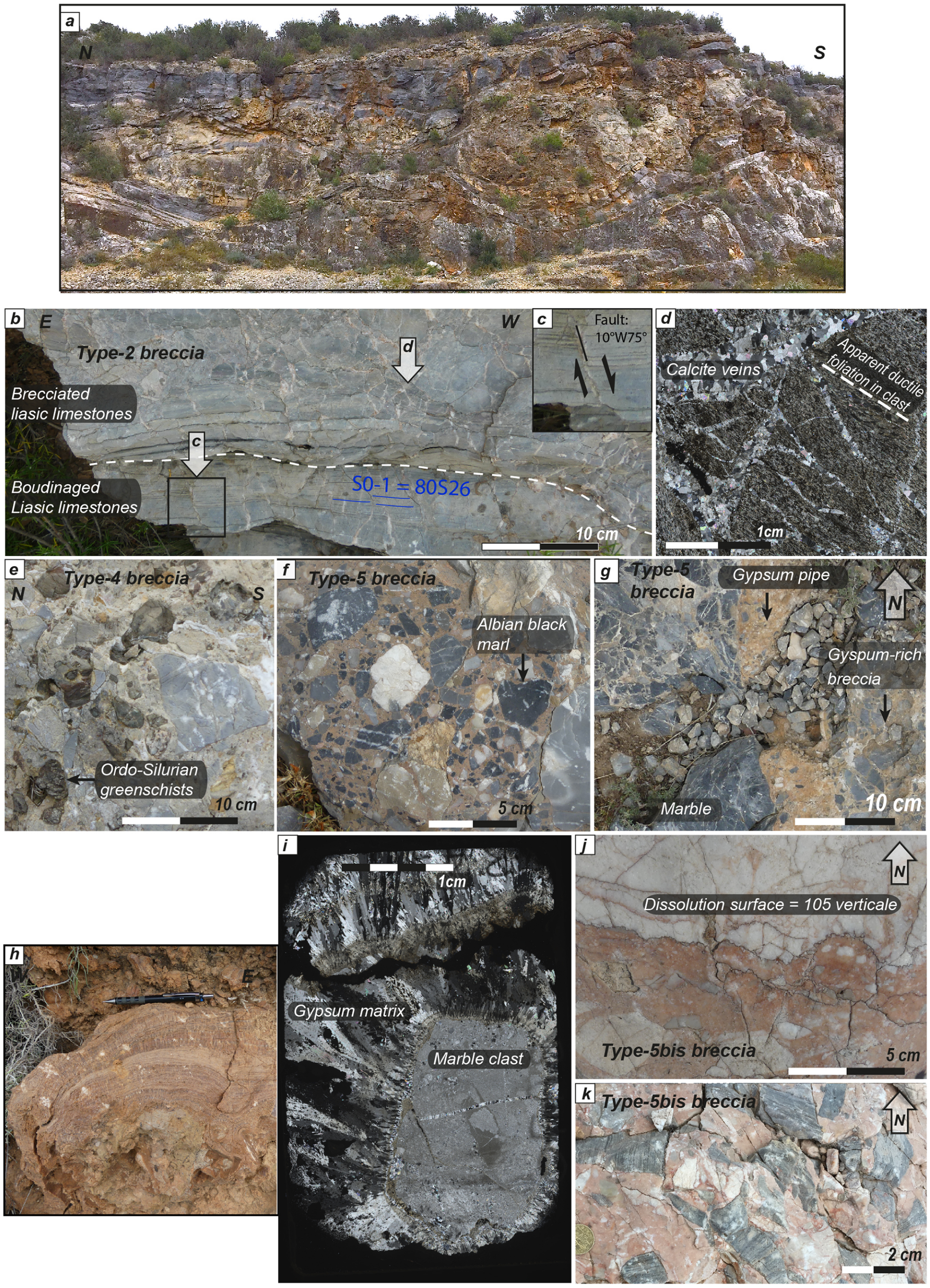

Fig. 11. A) Photograph of ductile boudinaged Early Jurassic marbles near Calce. B) Photograph illustrating the ductile-brittle deformation at the base of the Mesozoic cover (Early Jurassic marbles, YZ principal plane strain). Note the relationship between small-scale high-angle normal fault and calcite veins (C). D) Thin section of the type-2 breccia in the basal Lower Jurassic, highlighting the angular clasts of foliated marbles and the cement made of calcite cement. E) Photograph of the type-4 breccia in the Col de la Dona. F) Photograph of the type-5 breccia (polymictic facies). G) Photograph of a gypsum pipe that crosscuts the type-5 breccia (oligomictic facies). Note that the gypsum locally fills the matrix. H) Outcrop of gypsum at the base of the type-5 breccia system. I) Marble clast associated to gypsum-rich matrix (prismatic minerals with low relief) in type-5 breccia. J) Dissolved surface in the marbles of type-5bis breccia. K) Type-5bis breccia (oligomictic facies). Location in Figure 10a.

Fig. 11. *Illustrations des brèches du Bas-Agly (la localisation des images est indiquée sur la Fig. 10a). A) Photographie illustrant le boudinage des marbres du Jurassique inférieur au Sud-Ouest de Calce. B) Photographie illustrant la déformation fragile-ductile à la base de la couverture mésozoïque au Nord-Ouest de Calce (vue du plan de déformation principal YZ). C) Relations entre une faille et les veines de calcite. D) Lame mince d'une brèche de type-2 dans le Jurassique inférieur, montrant des clastes angulaires de marbres foliés et des ciments calcitiques. E) Photographie d'une brèche de type-4 au Col de la Dona. F) Photographie d'une brèche de type-5 avec le faciès polymictique. G) Photographie d'une brèche de type-5 avec le faciès oligomictique, recoupée par un dyke de gypse. H) Pointement de gypse à l'échelle de l'affleurement dans un système de brèches de type-5. I) Claste de marbre associé à une matrice riche en gypse dans une brèche de type-5. J) Surface dissoute dans les marbres d'une brèche de type-5bis. K) Faciès oligomictique d'une brèche de type-5bis.*

Table 1. Summary table of the main sedimentological, structural and petrographical characteristics recognized in the field for each type of breccias.
Tableau 1. *Synthèse des caractéristiques sédimentologiques, structurales et pétrologiques des différents types de brèches.*

Breccia type	Type-1	Type-2	Type-2bis	Type-3	Type-4	Type-5	Type-5bis
Related figures	5a–e, 6, 7c–e, 8d–h	5f-g, 7g, 8b-c, 11b–d	7f	9	11e	11f-i	11j-k
Thickness	50 to 100 m	10 to 20 m	< 5 m	250 m	5 m	200 to 300 m	< 10 m
Structure	In contact with the basement, *via* albitized fault zones	Intraformationnal in the deformed basal Lias	Same as type-1	Marks an extensional contact between basement and cover	Marks the contact between basement and cover	Intraformationnal in the Dogger- lower Cretaceous interval	Same as type-3, but following stratigraphic interfaces
Clasts origin	Pre-Aptian Mesozoic cover, Saint Arnac granite and its country-rocks	Liasis ductile deformed limestones	Same as type-1	Pre-Aptian Mesozoic cover, schists, granulites and migmatites	Lias, Trias and Paleozoic Schists	Triassic to Albian Mesozoic cover	Pre-Aptian Mesozoic cover
Texture	Matrix supported, local coarsening upward clasts distribution	Clasts supported	Same as type-1	Matrix supported	Matrix supported	Matrix supported	Matrix supported
Clasts morphology	Sub-angular to rounded, sub-spherical	Angular to very angular, flat	Same as type-1	Sub-angular to rounded, sub-spherical	Sub-angular to rounded, sub-spherical	Angular to sub-rounded, sub-spherical	Sub-angular to angular, flat
Matrix or cement nature	Particulate carbonate matrix, with clayey to fine sandy grain-size	Cement made of calcitic veins + coarse carbonate particle	Cement made of calcitic veins + coarse carbonate particle	Calcarenite and calcitic veins	Calcarenite and calcitic veins	Particulate carbonate matrix, with gypsum and calcictic veins	Carbonate mud

type-2bis follows a monomictic composition trend with abundant elongated angular clasts. The type-2bis only differs from the type-2 by a slightly higher diversity of clasts (Fig. 12b). The type-3/type-4 group is characterized by poorly sorted spherical angular clasts supported by mixed arenitic-calcitic cement. Type-3 is monomictic while type-4 is clearly polymictic.

The second cluster (type-5bis, type-5 and type-1) includes oligo- to poly-mictic breccias with subangular to rounded moderately to highly spherical clasts, supported by a carbonated matrix. Within this group, type-1 breccias show an exceptional variability of fabrics and clast composition. The type-5 breccias are similar to the ones of type-1 (except that they involve gypsum) but differ on a coarser matrix enclosing poorly sorted subangular clasts (Fig. 12b). The subcluster type-5bis is distinguished on the low roundness and the high angularity of the clasts.

Our field investigations lead to the definition of seven types of breccias. The statistical approach suggests to pair the type-2 with the type-2bis, and the type-3 with the type-4. Only the pair type-3/4 and type-5bis is considered as statistically similar by the One-way ANOSIM test, in spite of their similarity in the AHC and the PCOa, because of the low number of breccias included for these types in the analysis (Figs. 12b and 12c). Therefore, the quantitative analysis of the petrographical criteria validates five families of breccias (type-1, types-2/2bis, types-3/4, type-5 and type-5bis) revealing specific genetic processes.

6 Definition and timing of brecciation processes

6.1 Brecciation processes

6.1.1 Type-1 breccias: gravity-flow process

We have recognized in type-1 breccia coarsening-upward sequences delimited by erosion surfaces (Fig. 5a). These features are typical of gravity-driven transport of coarse sediments supported by fine matrix and interstitial water characteristic of gravity flows (*e.g.*, Takahashi, 1981; Festa *et al.*, 2019). In addition to this local observation, all type-1 facies are characterized by matrix- to clast-supported fabrics, in which clasts have various shapes, sizes, orientations and sphericities within a fine-grained clayey-silty carbonate matrix. The strong polymictic nature and the variability in the breccia fabrics complement these features to indicate hybrid gravity-flow processes (Haughton *et al.*, 2009), either triggered by slope influence (Pomar, 2001) or tectonic disturbance (Goldfinger, 2011).

6.1.2 Type-2 and type-2bis breccias: hydrofracturing

The intraformational nature of type-2 breccias with clasts embedded in the metamorphosed Early Jurassic limestones and often found parallel to the S_{0-1} of marbles indicates an *in situ* process of brecciation associated with little transport. The general aspect of this facies corresponds to the clast-supported "mosaic breccia" subdivision in the classification of fault breccias of Woodcock and Mort (2008). However, the very high concentration of calcite cements delimiting the clasts testifies for an intense fluid circulation during the brecciation process.

The structural continuity between the ductile foliation S_{0-1} and boudinage of marbles, and their subsequent fluid-assisted brittle deformation (shear fractures and veins that crosscut the ductile fabric, Figs. 11b and 11c) reflects a ductile-brittle continuum during thinning of the marbles until their brecciation. This is further suggested by the fact that fluid-assisted high angle normal faulting is sub-vertical to the foliation which confirms that brittle deformation operated while the rock layer was still horizontal. In addition, burial-related stylolites parallel to S_{0-1} are observed in the marble and the breccias, thus emphasizing that ductile and brittle shearing occurred during extension and prior to peak burial in the sedimentary basin. It must be noted that obliquity between some fluid-assisted high-angle normal faults dipping to the West (Figs. 11b and 11c) and the main direction of stretching deduced from ductile deformation suggests a component of flattening associated with vertical shortening during extension. We interpret type-2 breccias as reflecting a combination of hydrothermal activity, associated with an extensional deformation in a ductile-brittle continuum while the pre-rift cover was detached above the Triassic salt. This is consistent with the observation of gypsum locally exposed below the basal Early Jurassic rocks of the Bas-Agly. We view type-2bis breccias characterized by more than 50% of calcite cement in sedimentary type-1 breccias that was secondarily tectonically brecciated by the same hydraulic fracturing process, because it is essentially an *in situ* process.

6.1.3 Type-3 and type-4 breccias: basement-cover tectonic melange and tectonic brecciation

Type-3 breccias observed in Belesta represent a major fault zone between the basement and the Mesozoic cover (Fig. 9). As such it should be viewed as a major detachment that served as a drain for fluids, which explains the high concentration of calcite cement. The poor organization and mixing of highly heterometric clasts with shear fractures and cataclasites suggest these breccias form a tectonic mélange (*e.g.*, Festa *et al.*, 2019). Considering that brittle deformation dominates, its formation postdates the development of type-2 breccias and hydraulic brecciation. It is also possible that the embrittlement process observed in type-2 breccias corresponds to the first stages of formation of type-3 breccias. The fact that the Belesta mélange reworks granulite elements reveals a crustal-scale, and perhaps lithospheric-scale, detachment leading to mantle exhumation to the South of the Agly neck zone. This contact preserves kinematic indicators of extension in Belesta area that can be followed continuously from the Agly and Salvezines basement massif to the Boucheville basin to the west. There, the contact is a reverse fault (Fig. 1b; Chelalou *et al.*, 2016) and bodies of mantle peridotites are found juxtaposed on pre- and syn-rift rocks of the Boucheville syncline (Lagabrielle *et al.*, 2010).

Similarly to type-3 breccias, type-4 breccias observed in the Col de la Dona area are positioned at the contact between the basement (here the Ordovician-Silurian schists) and the Triassic-Lower Jurassic series (Fig. 10). However, at the contrary to type-3, breccias they rework only materials from these two structural units. They are chaotic breccias, with a percentage of large clasts between 30 and 60% and a coarse calcarenitic matrix associated with calcite cement that fits with the fault breccia characteristics (Woodcock and Mort, 2008). We interpret them as a brecciated contact between the Palaeozoic and the Mesozoic cover.

6.1.4 The type-5 breccias: dissolution-collapse

Despite their polymictic nature, the type-5 breccias in the Bas-Agly syncline do not show any criteria of sedimentary processes including the lack of apparent layered structure. Their close relationships with preserved evaporite suggest a genetic link with salt tectonics. The exposures gypsum in the form of small-scale slat-bearing convolute features and decimetric veins indeed indicate salt migration and brine circulation. Because they are located in an anticline core we suggest the breccias formed during the ascent (passive or reactive) of Triassic salt. Due to the very low strength of salt and high solubility with water (Jackson and Hudec, 2017), the dissolution of evaporitic strata within a sedimentary pile triggers the collapse of the overlying levels and leads to an intraformational dissolution-collapse brecciation (*e.g.*, Stanton, 1966; Friedman, 1997; Warren, 2006). This process is described in sedimentary basins that involve a significant amount of evaporites (*e.g.*, Eastern Mediterranean ridge [Kastens and Spiess, 1984]; Western Canada [Broughton, 2013]; Svalbard [Eliassen and Talbot, 2005]; Tunisia [Bouhlel *et al.*, 2016]; or South China [Leach *et al.*, 2017]).

The irregular shape of many clasts in type-5 breccias and of stratigraphic layers, here interpreted as dissolved surfaces, is a characteristic feature of collapse breccias (Friedman, 1997; Eliassen and Talbot, 2005). The "dissolution textures" seen in type-5 breccias can result from the dissolution of rocks either by the circulation of brines from the evaporitic level or by the circulation of subsurface water in a karst system that developed at the roof of the salt-wall.

6.1.5 The type-5bis breccias: karstic brecciation

The mono- to oligomictic type-5bis breccias of the Bas-Agly syncline, characterized by (sub)angular and nonspherical clasts aligned in a carbonate muddy matrix, can be interpreted as originated in a karstic network, as suggested by small voids between stratigraphic levels whose irregular walls strongly recall karren figures. Salt tectonics can generate large karst systems at the top of diapiric structures, as described for example in the Hormozgan province in Iran (*e.g.*, Bosák *et al.*, 1998, 1999). As the salt dissolves, the more the roof of the system is karstified, the more effective is the brecciation during collapse (Loucks, 1999; Loucks and Mescher, 2002). The lack of preserved cap rock, which marks the uppermost part of salt diapirs (Bosák *et al.*, 1998) made of Triassic to Albian clasts supports the collapse of the diapiric-karstic structure in the Bas-Agly syncline.

6.1.6 Outliers

Field observations and multivariate analysis of breccia resolve two main groups of breccias: on the one hand, tectonic (types-3/4) and fluid-assisted breccias (types-2/2bis), and, on the other hand, sedimentary (type-1), dissolution-collapse (type-5), and karstic breccias (type-5bis) (Fig. 12). Three samples however do not correspond to these main types although they fall in the range of the second cluster (sedimentary, karst and dissolution-collapse breccias). Sample BA95 (monogenic, angular, and jointed clasts), collected at the Roc de Lansac site within type-1 breccias (debris flow), is morphologically close to type-5bis breccias (karstic). This particular context likely indicates rock-fall processes, which can occur in both karst and debris flow systems. Similarly, type-5 features of the sample PRR4 issued from the type-1 breccia in Roquo Roujo may indicate processes of dissolution-collapse above the Agly Massif. On the opposite, the type-1 features of the type-5 sample PBC4, might mark the local development of debris-flow associated with the dissolution-collapse processes in the Bas-Agly.

6.2 Timing of brecciation processes: evidence for syn-rift Cretaceous emplacement of Agly breccias

We have established that the formation of the Agly breccias is the expression of tectonic, diapiric and sedimentary processes reworking the pre-Aptian sedimentary cover and the Paleozoic basement. *In situ* hydraulic fracturing documented at the base of the cover in the Agly Massif, mainly in the Lower Jurassic, appears to be linked to fluid-assisted brecciation and ductile-brittle extensional deformation. Structurally above, we have emphasized the relationship between salt tectonics and intra-cover brecciation in the Bas-Agly anticline. Most of the breccias recognized in the field show direct relationships with a major fluid and thermal event recorded in the pre-Aptian strata. Such a hydrothermal event is supported by the (1) occurrence of fluid-assisted tectonic brecciation (type-2 and type-2bis breccias), (2) the leaching of rocks in the Belesta mélange (type-3 breccias), and (3) the albitized contacts between cover or sedimentary breccias and basement (type-1 and type-4 breccias). The cover-basement contact is often found associated with extensional structures such as the albite-rich low-angle normal fault at the basement-cover interface (Roc de Lansac) and the asymmetric boudinage in the Belesta mélange zone. In the Bas Agly, it is argued that the vertical stress responsible for the ductile thinning and the fluid-assisted brecciation of the basal cover operated before the tilting or folding of the stratification. These observations support that breccias were associated with extensional deformation that occurred at a temperature above 300 °C most likely during the Pyrenean rifting as previously proposed by Vauchez *et al.* (2013) and Clerc *et al.* (2016).

The recent efforts in dating rift-related fluid events both in the cover and the basement offer us the opportunity to examine the age of emplacement of breccias. On the one hand, hydrothermalism in the basement is dated from the late Aptian in the SalvezinesMassif (117.5 ± 0.4 Ma, Boulvais *et al.*, 2007) to the early Cenomanian in the Agly Massif (albitization of the St-Arnac granites in the Agly Massif: 98 ± 2 Ma, Poujol *et al.*, 2010). Geochronological constraints from the Boucheville syncline, based on titanite found in a boudinaged sill, argue for deformation and metamorphism at 97 Ma (Chelalou *et al.*, 2016). On the other hand, fluid-related tectonics that occurred between 117 and 97 Ma suggest that hydraulic fracturing recognized at the base of the Mesozoic cover (type-2 breccias) developed during the same interval. The lack of clasts younger than the Aptian in the sedimentary type-1 breccia (Serre de

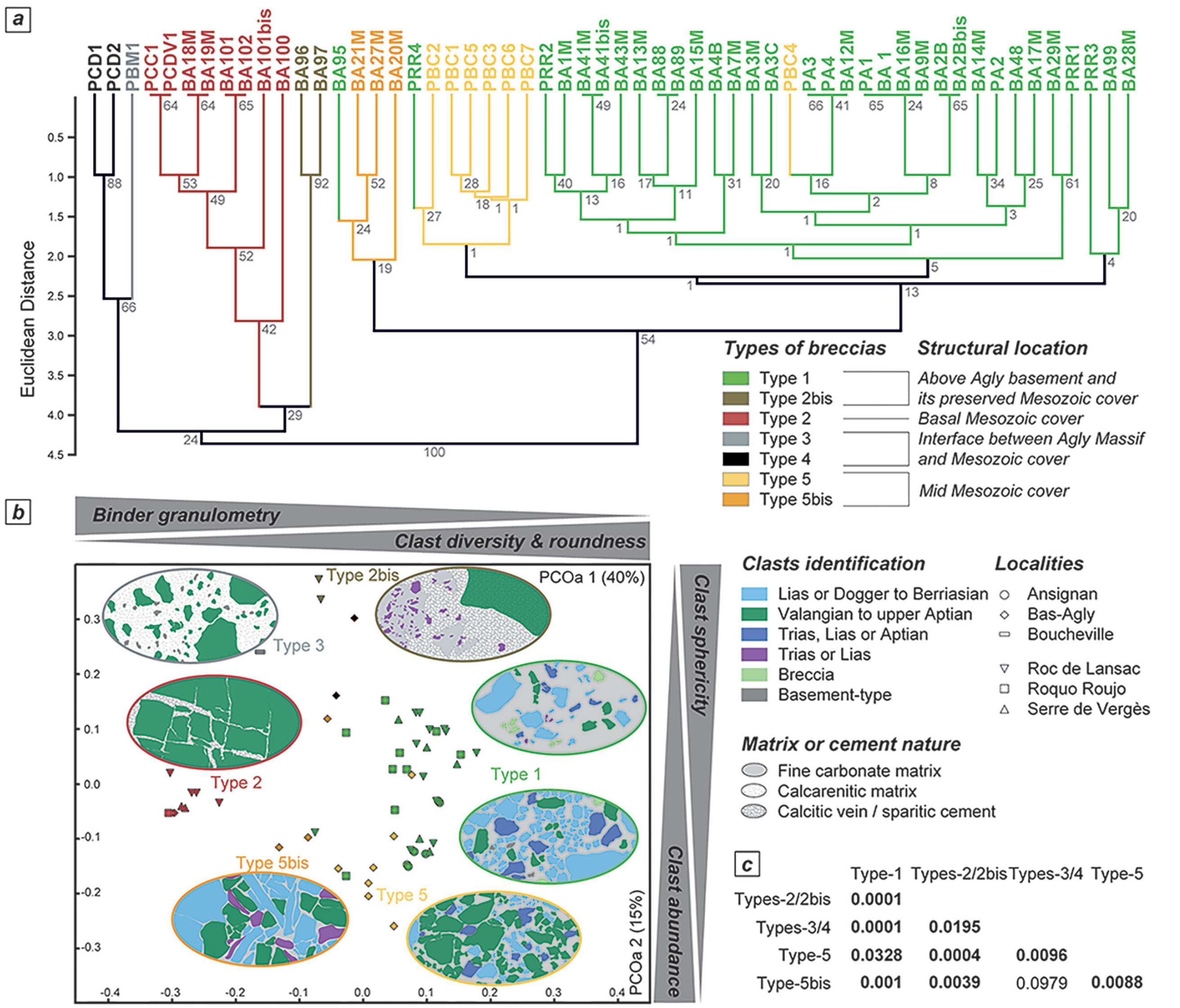

Fig. 12. Quantitative analysis of the petrographical characteristics of breccias (see Tab. 1 for uncategorized matrix). A) Agglomerative Hierarchical Clustering was obtained from the UPGMA algorithm and the Euclidean distance. Bootstrap values were obtained after 1000 replications. B) Principal Coordinates Analysis performed with the Gower distance, interpreted following the main descriptive characters contributing to the organisation of the petrographical space. C) One-way pairwise ANOSIM test validates significant differences between pairs of types of breccia ($p < 0.05$) except for types-3/4 and type-5bis (each represented by 3 samples). Samples are labelled according to their original location.

Fig. 12. *Analyses quantitatives des brèches, basée sur les critères présentés en tableau 1. A) Classification hiérarchique ascendante (distance euclidienne et méthode UPGMA). Les valeurs de bootstrap sont basées sur 1000 réplications. B) Analyse en coordonnées principales (à partir de la distance de Gower), montrant les principaux critères construisant l'espace pétrographique. C) Test de similarité entre les familles de brèches. Les paires de brèches sont significativement différentes sauf pour la paire types-3/4 et type-5bis dont le nombre d'échantillons étudié est insuffisant pour le test.*

Vergès, Roc de Lansac and Roquo Roujo) also supports brecciation processes occurring before the deposition and lithification of the Albian black flysch. We infer that the sedimentary breccias were deposited between the late Aptian and early Albian. Some preliminary U–Pb dates obtained on calcite from these breccias support this temporal scheme (Kernif *et al.*, 2020).

Halokinetic movements at the origin of type-5 and type-5bis breccias are thought to have been extremely limited until the Late Jurassic in the Pyrenees, as the thickness of the Jurassic deposits and tectonics was not sufficient to trigger instabilities in salt (Canérot and James, 1999; Canérot *et al.*, 2005). The Aptian-Albian time is a pivotal period in the Pyrenees that marks the onset of salt tectonics. This period reflects an increase of rift-related subsidence until a climax is reached during the deposition of the Albo-Cenomanian flysch (Canérot and Lenoble, 1993; Canérot and James, 1999; Canérot *et al.*, 2005; Duretz *et al.*, 2019; Labaume and Teixell, 2020; Ford and Vergés, 2021). Our observations from type-5 and type-5bis breccias agree with this regional subsidence

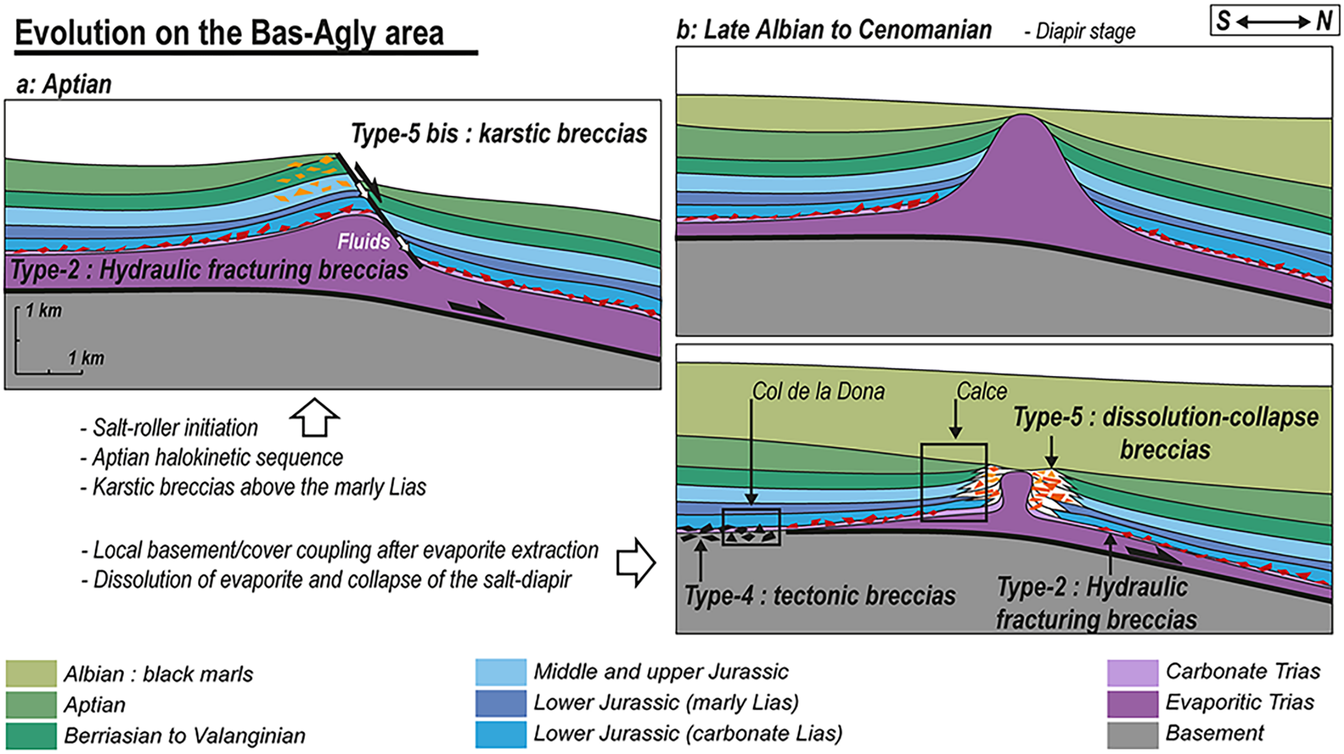

Fig. 13. Scheme showing the evolution of the Bas-Agly cover from Aptian to Cenomanian.
Fig. 13. *Schéma représentant l'évolution de la couverture du Bas-Agly de l'Aptien au Cénomanien.*

history on the European side of the Pyrenean rift and confirm that salt tectonics initiated during the early Cretaceous rifting.

The static recrystallization of the matrix observed in most breccias, even the notably less metamorphosed type-1 breccias, which rework previously metamorphosed and sheared limestones (mylonitized marbles) suggests temperatures were kept at a high level in the basin after brecciation and deposition (type-1 breccias). Syn-kinematic temperatures at the base of the detached cover in the Jurassic marbles on the southern flank of the Bas-Agly syncline reached 340–390 °C (Vauchez *et al.*, 2013), hence providing a qualitative estimate of the maximum temperatures reached by sediment cover above the Agly Massif. These temperatures are distinctively lower than those measured in Albian sediments from the adjacent basins of Boucheville and Bas-Agly. This is because local heat advection and depositional burial resulting from crustal thinning tend to increase towards the center of the basins where the younger sediments are deposited. This is a characteristic feature of the Pyrenean rift basins (*e.g.*, Clerc *et al.*, 2015; Ducoux *et al.*, 2019), which is predicted by numerical mechanical modeling of salt-related rifts (Duretz *et al.*, 2019; Jourdon *et al.*, 2020). This requires a high geothermal gradient up to 80 °C/km that can be maintained during the early stage of convergence because of continuous burial that compensates for thermal relaxation (Vacherat *et al.*, 2014). It results that mylonitized marbles may record brecciation as the salt is extracted while the temperature continuously increases or is kept stable over time. As a result, all breccias recorded heating rapidly after (type-2, type-3 and type-4 during the Aptian) or long after (type-1, type-5 and 5bis after burial below the Albo-Cenomanian sediments) the main episode of brecciation (and deposition *e.g.*, type-1).

6.3 Brecciation processes across rift domains

Figures 13 and 14 present a reconstruction of different parts of the European half-rift that integrates the formation of three main types of breccias. In these reconstructions we follow previous inferences (Clerc *et al.*, 2016; Ternois *et al.*, 2019; Ducoux *et al.*, 2021; Ford and Vergés, 2021) that positioned the area comprising the Bas-Agly syncline, Agly Massif and the Boucheville syncline at the transition between the necking zone and the distal rift domain. This inference is based on the strong metamorphic imprint observed in the pre- and syn-rift sediments. The Saint Paul de Fenouillet syncline, in contrast, represents a more proximal domain with a moderate thermal imprint. It should be noted that the maximum temperatures recorded in the syn-rift and pre-rift series (Fig. 1) imply temperature homogenisation in relation with fluid circulations, as has been demonstrated in the Boucheville basin (Boulvais, 2016).

In the Bas-Agly area (Fig. 13), we distinguish a first stage during which both the basement and the supra-salt cover are thinned above the Triassic salt that accommodates basement-cover decoupling. As the Triassic salt is progressively tectonically removed during the initial stage of extension deformation rate increases at the base of the cover. Pressure gradients in the originally weak and ductile salt décollement promoted fluid flows and embrittlement of the cover leading to hydrofracturing brecciation of the supra-salt cover (type-2

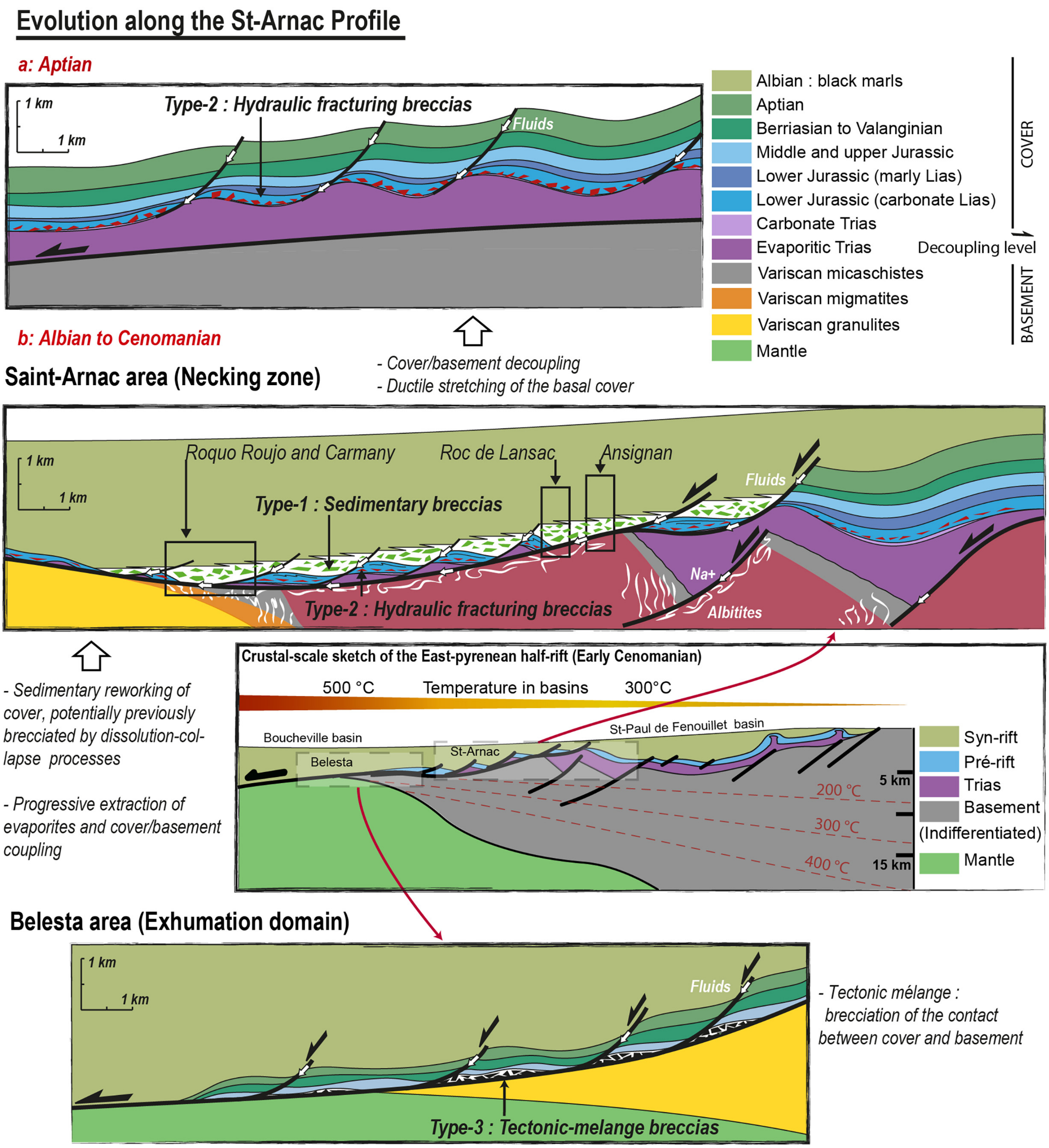

Fig. 14. Scheme representing the evolution of the European half-rift along the Saint Arnac profile that integrates the different breccias described and interpreted in this work. Note that the restauration of the rift is inspired by previous work (Ternois *et al.*, 2019: Clerc *et al.*, 2015) and our study. The isotherms in the basement of the paleorift are inspired from numerical modelling study (*e.g.*, Duretz *et al.*, 2019).

Fig. 14. *Reconstructions de la partie Européenne du demi-rift pyrénéen intégrant les différents types de brèches décrites et interprétées dans ce travail.*

breccias). Two additional and different configurations are associated through time with the formation of diapirs or salt pillows. First, as the sedimentary cover is faulted and salt rises at the initiation of Cretaceous rifting, karst can develop at the roof of the salt-core anticlines or salt-rollers (type-5bis breccias, Fig. 13a). Second, during the Albian-Cenomanian, as extension-related subsidence increases, the deposition of thick Albian flyschs triggers the vertical migration of salt (Ford and Vergés, 2021), and the diapiric structures progressively break through their overburden (gypsum pipes) and collapse at the origin of dissolution-collapse breccias (type-5 breccias, Fig. 13b). Finally, the regions where the salt has been fully extracted, as for example in the south of the Bas-Agly, are marked by cataclastic brecciation that reflects increasing mechanical coupling between the basement and the cover (type-4 breccias, Fig. 13b).

In contrast to the Bas-Agly where the role of the basement was indirectly inferred, breccias from the centre of the Agly Massif offer the opportunity to examine with more details the temporal evolution of the basement-cover coupling. First, we note the occurrence of the same type-2 hydraulic breccias in the supra-salt cover above Agly Massif. We infer that a similar initial brecciation process occurred in this domain, revealing a similar initial basement-cover decoupling in the salt layer (Fig. 14a).

Sedimentary type-1 breccias as documented in the Serre de Vergès, Roc de Lansac and Roquo Roujo are interpreted to reflect the onset of coupling between the pre-Aptian cover and the Paleozoic basement as the Triassic salt was progressively removed (Fig. 14b). The occurrence of clasts from the pre-Aptian cover and small remnants of cataclastic Paleozoic basement in these sedimentary breccias is intriguing as thermochronological constraints suggest that the basement was not at the surface. This is indicated by gneissic rocks collected near our type-1 breccias that yielded apatite U–Pb ages of 119–153 Ma (Odlum and Stockli, 2019) and modelling of zircon (U–Th)/He dates that collectively suggest this domain resided at temperature above 200 °C. Although a rapid episode of local surface exposure of the Variscan basement from below the pre-Aptian cover and reworking of the detachment fault system before the Albian cannot be excluded based on the current thermal constraints, we propose an alternative hypothesis. We suggest that the exposure of the Variscan basement below the pre-Aptian cover was concomitant with Triassic salt ascent through the cover hence dragging upwards rocks from the Paleozoic basement and the cover. These clasts are then remobilized by sedimentary process at on the seafloor. Increasing crustal thinning is consistent with the albitization of the St-Arnac pluton and its upper and lower country rocks at the vicinity of the major fault zones. The long-lasting fluid migration at the cover-basement boundary promotes hydraulic fracturing above the Triassic salt (type-2bis breccias), and later in the sedimentary breccias (type-1bis breccias). We infer that the Serre de Vergès and the Roc de Lansac breccias are located at the break-away of the detachment, while the Roquo Roujo site which contains more basement clasts perhaps represent a more distal part of the European half-rift located closer to the exhumed deeper crustal level (*e.g.*, granulite) exposed in the Agly Massif.

The Belesta tectonic mélange contains pre-Aptian clasts and distinctive elements of the Variscan basement including the granulitic crust (Fig. 14). The fact that Variscan granulites are reworked together with the sedimentary cover reveals the mélange formed in a later (at least after the initial cover-basement decoupling) and more mature stage of rifting between the southern Agly Massif and the Boucheville syncline. In addition, the stratigraphic ages of the tectonized rocks found across the mélange show a progressive younging pattern upwards, indicating it is a wide shear zone that developed mainly parallel to the original stratigraphic succession. Because peridotites are exposed in the Boucheville syncline that is in the same structural position but a few kilometres to the west of the Belesta shear zone, we infer that this major detachment exhumed the mantle between the Agly Massif and the Boucheville basin (Fig. 14). This conforms to some reconstructions that place the hyper-extended rifted domain in the Boucheville basin (*e.g.*, Vauchez *et al.*, 2013; Clerc *et al.*, 2015) although the detachment surface was not included in these previous reconstructions of the contact between the Agly Massif and the Boucheville basin. The dominant brittle deformation documented in the granulitic crust (and inferred from the serpentinized peridodites in Salvezines) across the Belesta detachment is analogous to the latest stage of crustal thinning when the upper crust is coupled to the lower crust, allowing the exhumation of the mantle, as suggested by seismic data from the Iberian margin (*e.g.*, Sutra and Manatschal, 2012). Observations from the Iberian margin also indicate that pre-rift strata are kept mechanically coupled to the basement above the detachment exhuming the mantle. This contrasts with our observations in the Agly Massif that suggest the contact between the pre-rift cover and the basement remains tectonically active during the whole extension process, notably in the hyper-extended part of the riftwhere the mantle is exhumed.

We see the domain of the Agly Massif as the necking zone (St-Arnac pluton) which is defined mechanically by the transition between the mechanically decoupled proximal rifted domain (Saint Paul de Fenouillet basin) and the coupled distal rifted domain (Boucheville basin) where the basement is exhumed (*e.g.*, Peron-Pinvidic *et al.*, 2013; Tugend *et al.*, 2015).

6.4 Evolution from salt-rich to salt-poor rift and exhumation processes during rifting

Our study of the breccias exposed in the Agly Massif emphasizes the first-order control played by the evolution of the weak Triassic salt on the tectonic relationships between the sedimentary cover and the exhumation of deep crustal levels during the Pyrenean rifting.

During the first stage of rifting that is referred to as the salt-rich rifted stage, the presence of thick salt promotes efficient basement-cover decoupling between the supra-salt cover and the Variscan basement and triggers the incipient mobilization of the salt (Fig 15a). Rift-related tectonic movement during the late Aptian resulted in the formation of salt pillows and salt-core anticlines at the top of which karstic systems developed. These structures, which can initially be found in many locations on the rift, later evolve into diapirs (*e.g.*, elongated salt walls) as the crust thins and the syn-rift sediments accumulate. The migration of salt diapir in the overburden ultimately leads to salt dissolution at the origin of

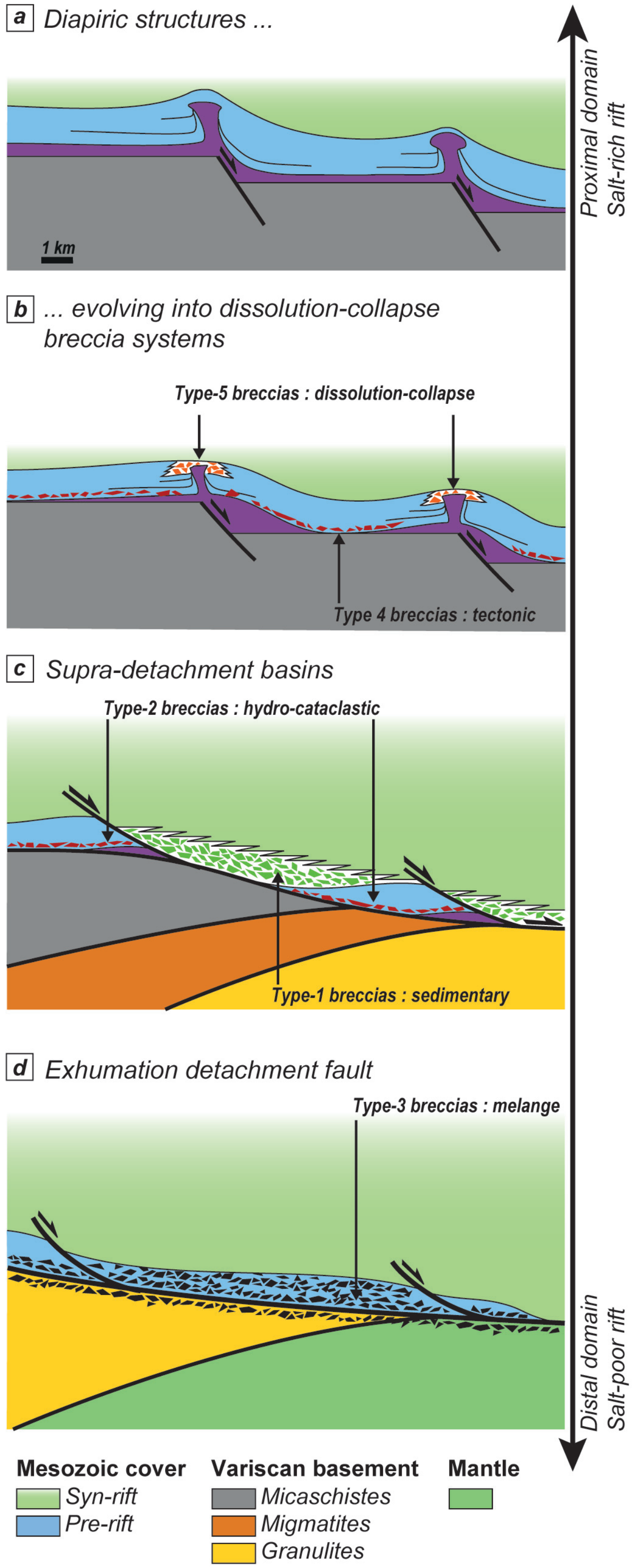

Fig. 15. Geological model placing the inferred brecciation processes in the context of a transition from salt-rich to salt-poor rift evolution as suggested for the formation of the rifted domains in the Agly Massif.

Fig. 15. *Modèles géologiques replaçant les processus de formation des brèches dans un système évoluant depuis un rift riche en évaporites jusqu'à un rift pauvre en évaporites.*

dissolution-collapse breccias (Fig. 15b). Faulting may locally occur in the basement and the cover but play a minor role in crustal thinning that is taken up by the decoupling between cover and basement. In our study region, this stage is well preserved on the southern flank of the Bas-Agly syncline, which reveals this domain escapes further deformation during ongoing extension (and possibly inversion).

As extension progresses the salt is extracted vertically through diapirism and laterally outwards from below the center of the subsident sag basins in the direction of lower pressure gradients. As the thickness of the viscous salt layer decreases the equivalent friction of the cover-basement interface increases. The rifting then enters into a salt-poor stage (Fig. 15c). The supra-salt cover is increasingly coupled to the basement along a low-angle detachment system rooting in the basement of the rift axis. This detachment that developed at the basement-cover interface during progressive extraction of the basement driving the subsequent steps of crustal extension on the distal rifted domain. This stage is reflected in the southern Agly Massif by the cooling history recorded in the Saint Arnac pluton and the granulitic rocks (*e.g.*, Odlum and Stockli, 2019). During this stage the principal mode of brecciation is associated to the dismantlement of the supra-salt cover, salt diapirism driving local sedimentary reworking at the surface combined with intense fluid-assisted tectonic brecciation of the top basement as observed in the Agly Massif, which arguably characterizes the evolution of the necking zone (Fig. 15c). As extension then migrates southward and localizes in the Boucheville basin during the Albian, the rift evolves towards a supra-detachment system (*e.g.*, Lavier and Manatschal, 2006; Sapin *et al.*, 2021), which hangingwall witnesses the exhumation and rotation of the lower crust and mantle and includes the previous mid-crustal detachment in a way similar to Jammes *et al.* (2009) (Fig. 14). Super-detachment basins are filled by syn-rift sediments, including sedimentary breccias (Friedmann and Burbank, 1995). However, in contrast to textbook example of supra-detachment extension models at magma-poor margins (*e.g.*, Iberia: Sutra and Manatschal, 2012), the main brittle exhumation system is located at the contact between the basement and the pre-rift cover as suggested by the Belesta mélange (Figs. 14 and 15d). The cover-basement limit, therefore, shapes a major and long-lived weak surface. This tectonic contact formed soon after rifting in the salt decollement. As extension increases salt remnants and high fluid pressure (hydrofracturing) collectively contributed to keep this cover-basement surface weak enough to allow the exhumation of lower crust and mantle in the distal rifted domain to upper crustal levels.

Our results agree partially with inference from other salt-rich basins of the Pyrenees like the Aulus basin or the Chainons Béarnais (Clerc *et al.*, 2012; Asti *et al.*, 2019; Lagabrielle *et al.*, 2019a, 2019b, 2020) in the sense that the salt décollement or some equivalent played a role in the exhumation of the mantle. However, it also differs from those models because 1) there is no evidence in support of gravitational sliding of the pre-rift cover towards the distal part of the rifted domain, 2) the exhumation in the distal rifted domain occurs in the brittle regime in agreement with Iberia-type model of extension on magma-poor margins (Sutra and Manatschal, 2012) and that 3) late stage of crustal thinning are characterized by exhumation of the crust and mantle.

7 Conclusion

In this paper our objective was to integrate the observation of breccias into the evolution of the basement-cover coupling in the development of rift-related Mesozoic basins of the Pyrenees. Our results demonstrate that the diversity of brecciation processes represent a rich and unique set of mechanisms (hydraulic fracturing, salt tectonics, basement exhumation) that is useful for reconstructing the spatio-temporal evolution crustal thinning across the rifted margins. Specifically, they allowed determining the timing and spatial evolution of coupling/decoupling processes across the basement-cover interface and how this relates to the late stage of exhumation of the mantle in the Pyrenees.

We propose for the first time a comprehensive study of breccias found dispersed in the eastern NPZ. A combination of petrologic and sedimentologic analyses, field-based structural study and multivariate analysis based on specific criteria (*e.g.*, clast shape, source, cement, thickness) allowed distinguishing 5 types of breccias, each associated with a particular brecciation process: 1) sedimentary breccias formed by the dismantlement of high angle normal fault scarps and deposition in supra-detachment basins, 2) tectonic breccias associated to cover-basement mechanical coupling/decoupling, 3) *in situ* hydraulic breccias associated to fluid flow accounting for overpressure along the decoupling level, 4) karstic brecciation above salt ridges associated to salt tectonics and 5) breccias related to dissolution and collapse of diapiric structures. The integration of these processes in the tectonic history of the eastern Pyrenees has led to the attribution of these breccias to Cretaceous rifting, resolving nearly 40 years of contradictory literature. We do not exclude that the cover-basement decoupling may have been reactivated but no data lend support for a Cenozoic origin for breccias. The minor role played by the salt layer during tectonic inversion is in line with the dominant thick-skinned style of shortening in the Agly Massif. The study of breccia systems has also highlighted the major role played by the evaporitic Triassic particularly during the first stages of rifting as a major decoupling level at the basement/cover interface on the necking zone of the rifted domain that later evolved as extension increases into a main detachment system leading to exhumation of deep crust and mantle. The long-term evolution of crustal thinning was accompanied by salt tectonics and shearing assisted by the circulation of fluids reflected in intense hydrofracturing of the base of the Mesozoic cover. The relationships between brecciation and Cretaceous extension in the Pyrenees argue for a mixed mode of rifting for the formation of hyper-extended rift. These models favor salt-controlled basement-cover decoupling in the first stage and brittle detachment faulting in the late stage.

Acknowledgement. This work was supported by CNRS-INSU-SYSTER research grants. We acknowledge Bryan Cochelin and an anonymous reviewer for their comments that significantly improved the quality of the manuscript. Romain Augier and Laurent Jolivet are thanked for their editorial handling.

References

Albarède F, Michard-Vitrac A. 1978a. Age and significance of the North Pyrenean metamorphism. *Earth and Planetary Science Letters* 104: 327–332.

Albarède F, Michard-Vitrac A. 1978b. Datation du métamorphisme des terrains secondaires des Pyrénées par les méthodes ^{39}Ar-^{40}Ar et ^{87}Rb-^{87}Sr. Ses relations avec les péridotites associées. *Bulletins de la société géologique de France* 20: 681–688.

Al Reda SM, Barbarand J, Gautheron C, Lasseur E, Loget N, Pinna-Jamme R, Briais J. 2021. Thermal record of the building of an orogen in the retro-foreland basin: Insight from basement and detrital thermochronology in the eastern Pyrenees and the North Pyrenean Basin (France). *Basin Research* 33(5): 2763–2791.

Althoff F, Barbey P, Pons J. 1994. La charnockite d'Ansignan et le granite de Saint-Arnac, témoins d'une extension crustale d'âge hercynien dans le massif de l'Agly (Pyrénées-Orientales, France). *Comptes rendus de l'Académie des sciences, série 2, sciences de la terre et des planètes* 319(2): 239–246.

Angrand P, Mouthereau F, Masini E, Asti R. 2020. A reconstruction of Iberia accounting for Western Tethys-North Atlantic kinematics since the late-Permian-Triassic. *Solid Earth* 11: 1313–1332.

Angrand P, Mouthereau F. 2021. Evolution of the Alpine orogenic belts in the Western Mediterranean region as resolved by the kinematics of the Europe-Africa diffuse plate boundary. *BSGF – Earth Sci Bull* 192(1): 42.

Asti R, Lagabrielle Y, Fourcade S, Corre B, Monié P. 2019. How do continents deform during mantle exhumation? Insights from the Northern Iberia inverted paleopassive margin, Western Pyrenees (France). *Tectonics* 38: 1666–1693.

Asti R, Rosseti F, Lucci F, Poujol M, Lagabrielle Y. 2021. Polyphase post-Variscan thinning of the North Pyrenean crust: Constraints from the P-T-t-deformation history of the exhumed Variscan lower crust (Saleix Massif, France). *Tectonophysics* 820: 229122.

Aumar C, Merle O, Bosse V, Monié P. 2022. Syn-rift Cretaceous deformation in the Variscan Agly Massif (Eastern Pyrenees, France). *BSGF - Earth Sci Bull* 193(6).

Azambre B, Rossy M. 1976. Le magmatisme alcalin d'âge crétacé, dans les Pyrénées occidentales et l'Arc basque; ses relations avec le métamorphisme et la tectonique. *Bulletin de la Société Géologique de France* S7(18): 1725–1728.

Barré G, Fillon C, Ducoux M, Mouthereau F, Gaucher EC, Calassou S. 2021. The North Pyrenean Frontal Thrust: structure, timing and late fluid circulation inferred from seismic and thermal-geochemical analyses of well data. *BSGF – Earth Sci. Bull.* 192(1): 52.

Bates RL, Jackson JA. 1980. Glossary of geology: falls church. Virginia: American Geological Institute, p. 167.

Beaumont C, Muñoz JA, Hamilton J, Fullsack P. 2000. Factors controlling the Alpine evolution of the central Pyrenees inferred from a comparison of observations and geodynamical models. *Journal of Geophysical Research: Solid Earth* 105: 8121–8145.

Berger GM, Alabouvette B, Bessière G, Bilotte M, Crochet B, Dubar M, Marchal JP, Tambareau Y, Villatte J, Viallard P. 1997. Carte géologique de la France à 1/50 000. 1078.

Berger GM, Fonteilles M, Leblanc D, Clauzon G, Marchal JP, Vautrelle C. 1993. Carte géologique de la France à 1/50 000. 1090.

Bernus-Maury C. 1984. Étude des paragéneses caractéristiques du métamorphime mésozoïque dans la partie orientale des Pyrénées. Thèse.

Bessière G, Bilotte M, Crochet B, Peybernès B, Tambareau Y, Villate J. 1989. Carte géologique de la France à 1/50 000. 1077.

Bilotte M, Bruxelles L, Canérot J, Laumonier B, Coinçon RS. 2007. Comment to "Latest-Cretaceous/Paleocene karsts with marine infillings from Languedoc (South of France): paleogeographic, hydrogeologic and geodynamic implications by P.J. Combes *et al.*". *Geodinamica Acta* 20: 403–413.

Blount DN, Moore CH. 1969. Depositional and non-depositional carbonate breccias, Chiantla Quadrangle, Guatemala. *GSA Bulletin* 80: 429–442.

Bosák P, Bruthans J, Filippi M, Svoboda T, Šmíd J. 1999. Karst and caves in salt diapirs, SE Zagros Mts. (Iran). *Acta Carsologica* 28.

Bosák P, Jaroš J, Spudil J, Sulovský P, Václavek V. 1998. Salt plugs in the Eastern Zagros, Iran: results of regional geological reconnaissance. *Geolines* 7.

Bouhallier H, Choukroune P, Ballèvre M. 1991. Structural evolution of the deep Hercynian crust: the example of the Agly Massif, eastern Pyrenees, France. *Comptes Rendus de l'Académie des Sciences* 312: 647–654.

Bouhlel S, Leach DL, Johnson CA, Marsh E, Salmi-Laouar S, Banks DA. 2016. A salt diapir-related Mississippi Valley-type deposit: the Bou Jaber Pb-Zn-Ba-F deposit, Tunisia: fluid inclusion and isotope study. *Miner Deposita* 51: 749–780.

Boulvais P. 2016. Fluid generation in the Boucheville Basin as a consequence of the North Pyrenean metamorphism. *Comptes Rendus Geoscience* 348: 301–311.

Boulvais P, Ruffet, G, Cornichet J, Mermet M, 2007. Cretaceous albitization and dequartzification of Hercynian peraluminous granite in the Salvezines Massif (French Pyrénées). *Lithos* 93: 89–106.

Broughton PL. 2013. Devonian salt dissolution-collapse breccias flooring the Cretaceous Athabasca oil sands deposit and development of lower McMurray Formation sinkholes, northern Alberta Basin, Western Canada. *Sedimentary Geology* 283: 57–82.

Cadenas P, Lescoutre R, Manatschal G, Fernández-Viejo G. 2021. The role of extensional detachment systems in thinning the crust and exhuming granulites: analogies between the offshore Le Danois High and the onshore Labourd Massif in the Biscay/ Pyrenean rifts. *BSGF – Earth Sci. Bull.* 192(1).

Canérot J. 2006. Réflexions sur la « révolution danienne » dans les Pyrénées. *Comptes Rendus Geoscience* 338: 658–665.

Canérot J, Bauer J, Bilotte M, Bourdillon C, Colin JP, Debroas EJ, Magniez F, Mediavilla F, Ternet Y. 2004. Sur la structure, l'âge et l'origine des « brèches de Bosmendiette » (Pyrénées-Atlantiques). *Comptes Rendus Geoscience* 336: 951–958.

Canérot J, Hudec M, Rockenbauch K., 2005. Mesozoic diapirism in the Pyrenean orogen: Salt tectonics on a transform plate boundary. *AAPG Bulletin* 89: 211–229.

Canérot J, James V. 1999. Diapirism and post-Triassic structural development of the western Pyrenees and southern Aquitaine. *Eclogae Geol. Helv.* 92: 63–72.

Canérot J, Lenoble JL. 1993. Diapirisme crétacé sur la marge ibérique des Pyrénées occidentales ; exemple du pic de Lauriolle ; comparaisons avec l'Aquitaine, les Pyrénées centrales et orientales. *Bulletin de la Société Géologique de France* 164: 719–726.

Cathelineau M, Boiron MC, Jakomulski H. 2021. Triassic evaporites: a vast reservoir of brines mobilized successively during rifting and thrusting in the Pyrenees. *Journal of the Geological Society*.

Chelalou R. 2015. Formation et évolution du bassin de Boucheville, implication sur l'évolution tectonique, métamorphique et sédimentaires des bassins sédimentaires mésozoïques du Nord-Est des Pyrénées. Thèse.

Chelalou R, Nalpas T, Bousquet R, Prevost M, Lahfid A, Poujol M, Ringenbach JC, Ballard JF. 2016. New sedimentological, structural and paleo-thermicity data in the Boucheville Basin (eastern North Pyrenean Zone, France). *Comptes Rendus Geoscience, From rifting to mountain building: the Pyrenean Belt* 348: 312–321.

Choukroune P. 1989. The Ecors Pyrenean deep seismic profile reflection data and the overall structure of an orogenic belt. *Tectonics* 8: 23–39.

Choukroune P, Roure F, Pinet B. 1990. Main results of the ECORS Pyrenees profile. *Tectonophysics, Siesmic Probing of Continents and their Margins* 173: 411–423.

Clarke KR. 1993. Non-parametric multivariate analysis of changes in community structure. *Australian Journal of Ecology* 18: 117–143.

Clerc C. 2012. Évolution du domaine nord-pyrénéen au Crétacé : amincissement crustal extrême et thermicité élevée : un analogue pour les marges passives. Thèse.

Clerc C, Lagabrielle Y. 2014. Thermal control on the modes of crustal thinning leading to mantle exhumation: Insights from the Cretaceous Pyrenean hot paleomargins. *Tectonics* 33: 1340–1359.

Clerc C, Lagabrielle Y, Labaume P, Ringenbach JC, Vauchez A, Nalpas T, Bousquet R, Ballard JF, Lahfid A, Fourcade S. 2016. Basement - Cover decoupling and progressive exhumation of metamorphic sediments at hot rifted margin. Insights from the northeastern Pyrenean analog. *Tectonophysics* 686: 82–97.

Clerc C, Lagabrielle Y, Neumaier M, Reynaud JY, de Saint Blanquat M. 2012. Exhumation of subcontinental mantle rocks: evidence from ultramafic-bearing clastic deposits nearby the Lherz peridotite body, French Pyrenees. *Bulletin de la Société Géologique de France* 183: 443–459.

Clerc C, Lahfid A, Monié P, Lagabrielle Y, Chopin C, Poujol M, Boulvais P, Ringenbach JC, Masini E, de Saint Blanquat M. 2015. High-temperature metamorphism during extreme thinning of the continental crust: a reappraisal of the North Pyrenean passive paleomargin. *Solid Earth* 6: 643–668.

Cohen KM, Finney SC, Gibbard PL, Fan JX, 2013. The ICS International Chronostratigraphic Chart. *Episodes* 36: 199–204.

Combes PJ. 1990. Typology, geodynamic context and genesis of french bauxites. *Geodinamica Acta* 4: 91–109.

Corre B, Boulvais P, Boiron MC, Lagabrielle Y, Marasi L, Clerc C. 2018. Fluid circulations in response to mantle exhumation at the passive margin setting in the north Pyrenean zone, France. *Mineralogy and Petrology* 112: 1–24.

Corre B, Lagabrielle Y, Labaume P, Fourcade S, Clerc C, Ballèvre M. 2016. Deformation associated with mantle exhumation in a distal, hot passive margin environment: New constraints from the Saraillé Massif (Chaînons Béarnais, North-Pyrenean Zone). *Comptes Rendus Geoscience, From rifting to mountain building: the Pyrenean Belt* 348: 279–289.

Dauteuil O, Ricou LE. 1989. Hot-fluid circulation as an origin for the North Pyrenean cretaceous metamorphism. *Geodinamica Acta* 3: 237–249.

Davis JC. 1986. Statistics and data analysis in geology. New York: John Wiley & Sons, 646 p.

de Saint Blanquat M, Bajolet F, Grand'Homme A, Proietti A, Zanti M, Boutin A, Clerc C, Lagabrielle Y, Labaume P. 2016. Cretaceous mantle exhumation in the central Pyrenees: New constraints from the peridotites in eastern Ariège (North Pyrenean zone, France). *Comptes Rendus Geoscience, From rifting to mountain building: the Pyrenean Belt* 348: 268–278.

Debroas EJ. 1990. Le flysch noir albo-cénomanien témoin de la structuration albienne a senonienne de la Zone nord-pyrénéenne en Bigorre (Hautes-Pyrénées, France). *Bulletin de la Société Géologique de France* 6: 273–285.

Debroas EJ. 1987. Modèle de bassin triangulaire a l'intersection de décrochements divergents pour le fosse albo-cenomanien de la Ballongue (zone nord-pyrénéenne, France). *Bulletin de la Société Géologique de France* 3: 887–898.

Debroas EJ. 1985. Géométrie et position structurale des fossés albiens nord-pyrénéens : l'exemple des Pyrénées centrales. *Strata* 1 (2): 99–106.

Delay F. 1989. Le massif nord-pyrénéen de l'Agly (Pyrénées orientales) : évolution tectono-métamorphique et exemple d'un amincissement crustal polyphasé. Thèse.

Desreumaux C, Clément B, Fabre R, Martins-Campina B. 2002. Découverte de turbidites du Crétacé supérieur métamorphisées au contact d'intrusions d'ophites dans les Pyrénées occidentales (vallée d'Aspe, France). Vers une révision de l'âge des ophites pyrénéennes. *Comptes Rendus Geoscience* 334: 197–203.

Ducoux M, Jolivet L, Callot JP, Aubourg C, Masini E, Lahfid A, Homonnay E, Cagnard F, Gumiaux C, Baudin T. 2019. The nappe des marbres unit of the Basque-Cantabrian Basin: The tectono-thermal evolution of a fossil hyperextended rift basin. *Tectonics* 38: 3881–3915.

Ducoux M, Jolivet L, Masini E, Augier R, Lahfid A, Bernet M, Calassou S. 2021. Distribution and intensity of high-temperature low-pressure metamorphism across the Pyrenean-Cantabrian belt: constraints on the thermal record of the pre-orogenic hyperextension rifting. *BSGF – Earth Sci Bull.* 192: 43.

Ducoux M, Jolivet L, Cagnard F, Baudin T. 2021. Basement-cover decoupling during the inversion of a hyperextended basin: insights from the eastern Pyrenees. *Tectonics* 40(5).

Duretz T, Asti R, Lagabrielle Y, Brun JP, Jourdon A, Clerc C, Corre B. 2019. Numerical modelling of Cretaceous Pyrenean Rifting: The interaction between mantle exhumation and syn-rift salt tectonics. *Basin Research* 32: 652–667.

Eliassen A, Talbot MR. 2005. Solution-collapse breccias of the Minkinfjellet and Wordiekammen Formations, Central Spitsbergen, Svalbard: a large gypsum palaeokarst system. *Sedimentology* 52: 775–794.

Esquevin J, Fournie D, Lestang J. 1971. L'Aptien et l'Albien nord-pyrénéens et sud-aquitains. *Bull. Centre Rech. S.N.P.A. Pau* 5: 87–151.

Festa A, Pini GA, Ogata K, Dilek Y. 2019. Diagnostic features and field-criteria in recognition of tectonic, sedimentary and diapiric mélanges in orogenic belts and exhumed subduction-accretion complexes. *Gondwana Res* 74: 7–30.

Fillon C, Mouthereau F, Calassou S, Pik R, Bellahsen N, Gautheron C, Stockli D, Brichau S, Daril N, Mouchené M, van der Beek P. 2021. Post-orogenic exhumation in the western Pyrenees: evidence for extension driven by pre-orogenic inheritance. *J Geol Soc London* 178.

Folk RL, Ward WC. 1957. Brazos River bar [Texas]; a study in the significance of grain size parameters. *Journal of Sedimentary Research* 27: 3–26.

Fonteilles M, Leblanc D, Clauzon G, Vaudin JL, Berger GM. 1993. Carte géologique de la France (1/50 000), feuille Rivesaltes (1090). Orléans : BRGM.

Ford M, Vergés J. 2021. Evolution of a salt-rich transtensional rifted margin, eastern North Pyrenees, France. *Journal of the Geological Society* 178(1).

Friedman GM. 1997. Dissolution-collapse breccias and paleokarst resulting from dissolution of evaporite rocks, especially sulfates. *Carbonates Evaporites* 12: 53–63.

Friedmann SJ, Burbank DW. 1995. Rift basins and supradetachment basins: intracontinental extensional end-members. *Basin Research* 7: 109–127.

Gale AS, Mutterlose J, Batenburg S, Gradstein FM, Arterberg FR, Ogg JG, Petrizzo MR. 2020. The Cretaceous Period. 1023–1086. In: Gradstein FM, Ogg J, Schmitz MD, Ogg GM, eds. Geological Time Scale, 2020, vol. 2.

Gawthorpe RL, Leeder MR. 2000. Tectono-sedimentary evolution of active extensional basins. *Basin Research* 12: 195–218.

Golberg JM. 1987. Le métamorphisme mésozoïque dans la partie orientale des Pyrénées : relations avec l'évolution de la chaîne au Crétacé. Thèse.

Golberg JM, Leyreloup AF. 1990. High temperature-low pressure Cretaceous metamorphism related to crustal thinning (Eastern North Pyrenean Zone, France). *Contr. Mineral. Petrol.* 104: 194–207.

Golberg JM, Maluski H. 1988. Données nouvelles et mise au point sur l'âge du métamorphisme pyrénéen. *C. R. Acad. Sci., Sér. 2, Méc. Phys. Chim. Sci. Univers Sci. Terre* 306: 429–435.

Golberg JM, Maluski H, Leyreloup AF. 1986. Petrological and age relationship between emplacement of magmatic breccia, alkaline magmatism, and static metamorphism in the North Pyrenean Zone. *Tectonophysics, The Geological Evolution of the Pyrenees* 129: 275–290.

Goldfinger C. 2011. Submarine paleoseismology based on turbidite records. *Ann. Rev. Mar. Sci.* 3: 35–66.

Grool A, Huismans R, Ford M. 2019. Salt décollement and rift inheritance controls on crustal deformation in orogens. *Terra Nova* 31.

Gower JC. 1966. Some distance properties of latent root and vector methods used in multivariate analysis. *Biometrika* 53(3–4): 325–338.

Hammer Ø, Harper DA, Ryan PD. 2001. PAST: Paleontological statistics software package for education and data analysis. *Palaeontologia Electronica* 4(1): 9.

Haughton P, Davis C, McCaffrey W, Barker S. 2009. Hybrid sediment gravity flow deposits - classification, origin and significance. *Marine and Petroleum Geology* 26: 1900–1918.

Incerpi N, Manatschal G, Martire L, Bernasconi SM, Gerdes A, Bertok C. 2020a. Characteristics and timing of hydrothermal fluid circulation in the fossil Pyrenean hyperextended rift system: new constraints from the Chaînons Béarnais (West Pyrenees). *Int J Earth Sci (Geol Rundsch)* 109: 1071–1093.

Incerpi N, Martire L, Manatschal G, Bernasconi SM, Gerdes A, Czuppon G, Palcsu L, Karner G, Johnson CA, Figueredo PH. 2020b. Hydrothermal fluid flow associated to the extensional evolution of the Adriatic rifted margin: Insights from the pre- to post-rift sedimentary sequence (SE Switzerland, N ITALY). *Basin Research* 32: 91–115.

Jackson MPA, Hudec MR. 2017. Salt tectonics: principles and practice. Cambridge University Press.

Jaffrezo M. 1980. Les formations carbonatées des Corbières (France) du Dogger à l'Aptien : micropaléontologie stratigraphique, biozonation, paléoécologie, extension des résultats à la Mésogée. Thèse.

Jammes S, Huismans RS. 2012. Structural styles of mountain building: Controls of lithospheric rheologic stratification and extensional inheritance. *J. Geophys. Res.* 117.

Jammes S, Manatschal G, Lavier L. 2010. Interaction between prerift salt and detachment faulting in hyperextended rift systems: The example of the Parentis and Mauléon basins (Bay of Biscay and western Pyrenees). *AAPG Bulletin* 94: 957–975.

Jammes S, Manatschal G, Lavier L, Masini E. 2009. Tectonosedimentary evolution related to extreme crustal thinning ahead of a propagating ocean: Example of the western Pyrenees. *Tectonics* 28 (4).

Jébrak M. 1997. Hydrothermal breccias in vein-type ore deposits: A review of mechanisms, morphology and size distribution. *Ore Geology Reviews* 12: 111–134.

Jourdon A, Le Pourhiet L, Mouthereau F, Masini E. 2019. Role of rift maturity on the architecture and shortening distribution in mountain belts. *Earth and Planetary Science Letters* 512: 89–99.

Jourdon A, Mouthereau F, Pourhiet LL, Callot JP. 2020. Topographic and tectonic evolution of mountain belts controlled by salt thickness and rift architecture. *Tectonics* 39.

Kastens KA, Spiess FN. 1984. Dissolution and collapse features on the eastern Mediterranean Ridge. *Marine Geology* 56: 181–193.

Kernif T, Nalpas T, Bourquin S, Gautier P, Poujol M. 2021. Sedimentary breccias formed during extensional tectonics: facies organization and processes. In: EGU General Assembly Conference Abstracts. pp. EGU21–5681.

Kernif T, Nalpas T, Gautier P, Bourquin S, Poujol M. 2020. Formation and preservation of syntectonic sedimentary breccias in extensional environments (Crete and Pyrenees) and in situ U-Pb constraints for the age of breccias in the Bas-Agly Basin. In: EGU General Assembly Conference Abstracts. pp. 9024.

Krumbein WC, Sloss LL. 1964. Stratigraphy and Sedimentation. *Bulletin de Minéralogie* 87(124).

Labaume P, Teixell A. 2020. Evolution of salt structures of the Pyrenean rift (Chaînons Béarnais, France): From hyper-extension to tectonic inversion. *Tectonophysics* 785: 228451.

Lagabrielle Y, Asti R, Duretz T, Clerc C, Fourcade S, Teixell A, Labaume P, Corre B, Saspiturry N. 2020. A review of cretaceous smooth-slopes extensional basins along the Iberia-Eurasia plate boundary: How pre-rift salt controls the modes of continental rifting and mantle exhumation. *Earth-Science Reviews* 201.

Lagabrielle Y, Asti R, Fourcade S, Corre B, Labaume P, Uzel J, Clerc C, Lafay R, Picazo S. 2019a. Mantle exhumation at magma-poor passive continental margins. Part II: Tectonic and metasomatic evolution of large-displacement detachment faults preserved in a fossil distal margin domain (Saraillé lherzolites, northwestern Pyrenees, France). *Bulletin de la Société Géologique de France* 190.

Lagabrielle Y, Asti R, Fourcade S, Corre B, Poujol M, Uzel J, Labaume P, Clerc C, Lafay R, Picazo S, Maury R. 2019b. Mantle exhumation at magma-poor passive continental margins. Part I. 3D architecture and metasomatic evolution of a fossil exhumed mantle domain (Urdach lherzolite, north-western Pyrenees, France). *Bulletin de la Société Géologique de France* 190.

Lagabrielle Y, Bodinier JL. 2008. Submarine reworking of exhumed subcontinental mantle rocks: field evidence from the Lherz peridotites, French Pyrenees. *Terra Nova* 20: 11–21.

Lagabrielle Y, Clerc C, Vauchez A, Lahfid A, Labaume P, Azambre B, Fourcade S, Dautria JM. 2016. Very high geothermal gradient during mantle exhumation recorded in mylonitic marbles and carbonate breccias from a Mesozoic Pyrenean palaeomargin (Lherz area, North Pyrenean Zone, France). *Comptes Rendus Geoscience*, *From rifting to mountain building: the Pyrenean Belt* 348: 290–300.

Lagabrielle Y, Labaume P, de St. Blanquat M. 2010. Mantle exhumation, crustal denudation, and gravity tectonics during Cretaceous rifting in the Pyrenean realm (SW Europe): Insights from the geological setting of the lherzolite bodies. *Tectonics* 29: 1–26.

Lavier LL, Manatschal G. 2006. A mechanism to thin the continental lithosphere at magma-poor margins. *Nature* 440: 324–328.

Laznicka P. 1989. Breccias and ores. Part 1: History, organization and petrography of breccias. *Ore Geology Reviews* 4: 315–344.

Leach DL, Song YC, Hou ZQ. 2017. The world-class Jinding Zn-Pb deposit: ore formation in an evaporite dome, Lanping Basin, Yunnan, China. *Miner Deposita* 52: 281–296.

Leeder MR, Gawthorpe RL. 1987. Sedimentary models for extensional tilt-block/half-graben basins. *Geological Society, London, Special Publications* 28: 139–152.

Lister GS, Davis GA. 1989. The origin of metamorphic core complexes and detachment faults formed during Tertiary continental extension in the northern Colorado River region, U.S.A. *Journal of Structural Geology* 11: 65–94.

Loucks RG, Mescher PK. 2002. Paleocave facies classification and associated pore types. *AAPG Bulletin* 1–18.

Loucks RG. 1999. Paleocave carbonate reservoirs: origins, burial-depth modifications, spatial complexity, and reservoir implications. *AAPG Bulletin* 83(11): 1795–1834.

Masini E, Manatschal G, Tugend J, Mohn G, Flament JM. 2014. The tectono-sedimentary evolution of a hyper-extended rift basin: the example of the Arzacq-Mauléon rift system (Western Pyrenees, SW France). *Int J Earth Sci* 103: 1569–1596.

Mattauer M, Proust F. 1962. Sur l'age post-Albien de quelques brèches réputées jurassiques ou néocomiennes des Pyrénées Orientales. *Comptes Rendus de la Société Géologique de France* 10: 304–305.

Montigny R, Azambre B, Rossy M, Thuizat R. 1986. K-Ar Study of cretaceous magmatism and metamorphism in the pyrenees: Age and length of rotation of the Iiberian Peninsula. *Tectonophysics, The Geological Evolution of the Pyrenees* 129: 257–273.

Morrow DW. 1982. Descriptive field classification of sedimentary and diagenetic breccia fabrics in carbonate rocks. *Bulletin of Canadian Petroleum Geology* 30: 227–229.

Motte G, Hoareau G, Callot JP, Révillon S, Piccoli F. Calassou S, Gaucher EC. 2021. Rift and salt-related multi-phase dolomitization: example from the northwestern Pyrenees. *Marine and Petroleum Geology* 126: 104932.

Mouthereau F, Filleaudeau PY, Vacherat A, Pik R, Lacombe O, Fellin MG, Castelltort S, Christophoul F, Masini E. 2014. Placing limits to shortening evolution in the Pyrenees: Role of margin architecture and implications for the Iberia/Europe convergence: Plate convergence in the Pyrenees. *Tectonics* 33: 2283–2314.

Mouthereau F, Angrand P, Jourdon A, Ternois S, Fillon C, Calassou S, Chevrot S, Ford M, Jolivet L, Manatschal G, Masini E, Thinon I, Vidal O, Baudin T. 2021. Cenozoic mountain building and topographic evolution in Western Europe: impact of billions of years of lithosphere evolution and plate kinematics. *BSGF – Earth Sci Bulletin* 192(56).

Mukonzo JN, Boiron MC, Lagabrielle Y, Cathelineau M, Quesnel B. 2020. Fluid-rock interactions along detachment faults during continental rifting and mantle exhumation: the case of the Urdach lherzolite body (North-Pyrenees). *Journal of the Geological Society* 172(2).

Muñoz JA. 1992. Evolution of a continental collision belt: ECORS-Pyrenees crustal balanced cross-section. In: McClay KR, ed. Thrust tectonics. Dordrecht: Springer Netherlands, pp. 235–246.

Odlum ML, Stockli DF. 2019. Thermotectonic evolution of the North Pyrenean Agly Massif during early cretaceous hyperextension using multi-mineral U-Pb thermochronometry. *Tectonics* 38: 1509–1531.

Olivier P, Gleizes G, Paquette JL, Muñoz Sáez C. 2008. Structure and U-Pb dating of the Saint Arnac pluton and the Ansignan charnockite (Agly Massif): a cross-section from the upper to the middle crust of the Variscan Eastern Pyrenees. *Journal of the Geological Society* 165: 141–152.

Olivier Ph, Gleizes G, Paquette JL. 2004. Gneiss domes and granite emplacement in an obliquely convergent regime: New interpretation of the Variscan Agly Massif (Eastern Pyrenees France). In: Gneiss domes in Orogeny. Geological Society of America.

Ortí F, Pérez-López A, Salvany JM. 2017. Triassic evaporites of Iberia: Sedimentological and palaeogeographical implications for the western Neotethys evolution during the Middle Triassic-Earliest

Jurassic. *Palaeogeography, Palaeoclimatology, Palaeoecology* 471: 157–180.

Paquet J, Mansy JL. 1992. Evolution alpine du massif nord-pyrénéen de l'Agly (Pyrénées-Orientales). *C. R. Acad. Sci., Sér. 2, Méc. Phys. Chim. Sci. Univers Sci. Terre* 315: 487–494.

Paquet J, Mansy JL. 1991. La structure de l'Est des Pyrénées (transversales du massif de l'Agly) : un exemple d'amincissement crustal. *C. R. Acad. Sci., Sér. 2, Méc. Phys. Chim. Sci. Univers Sci. Terre* 312: 913–919.

Peacock DCP, Rotevatn A, Sanderson DJ. 2019. Brecciation driven by changes in fluid column heights. *Terra Nova* 31: 76–81.

Peron-Pinvidic G, Manatschal G, Osmundsen PT. 2013. Structural comparison of archetypal Atlantic rifted margins: A review of observations and concepts. *Marine and Petroleum Geology* 43: 21–47.

Peybernès, B. 1979. L'Urgonien des Pyrénées; Essai de synthèse. *Geobios, Mémoire spécial* 3: 79–87.

Peybernès B. 1978a. Le Jurassique des Pyrénées navarro-languedociennes.

Peybernès B. 1978b. Le Complexe Urgonien dans les Pyrénées navarro-languedociennes et catalanes.

Peybernès B. 1976. Le Jurassique et le Crétacé inférieur des Pyrénées franco-espagnoles entre la Garonne et la Méditerranée. Thèse.

Peybernès B, Fondecave-Wallez MJ, Combes PJ. 2002. Découverte de Foraminifères planctoniques paléocènes dans les brèches, précédemment tenues pour aptiennes et d'origine diapirique, des Pyrénées basco-béarnaises. *Comptes Rendus Palevol* 1: 3–10.

Peybernès B, Fondecave-Wallez MJ, Combes PJ, Eichène P. 2001a. Découverte d'hémipélagites à Foraminifères planctoniques paléocènes dans les « brèches de Baixas » (Pyrénées orientales). *Comptes Rendus de l'Académie des Sciences – Series IIA – Earth and Planetary Science* 332: 633–640.

Peybernès B, Fondecave-Wallez MJ, Combes PJ, Eichène P. 2001b. Mise en évidence d'un sillon marin à brèches paléocènes dans les Pyrénées centrales (Zone interne métamorphique et Zone nord-pyrénéenne). Comptes Rendus de l'Académie des Sciences – Series IIA – Earth and Planetary Science 332: 379–386.

Peybernès B, Souquet P. 1984. Basement blocks and tecto-sedimentary evolution in the Pyrenees during Mesozoic times. *Geological Magazine* 121: 397–405.

Pomar L. 2001. Types of carbonate platforms: a genetic approach. *Basin Research* 13: 313–334.

Poujol M, Boulvais P, Kosler J. 2010. Regional-scale Cretaceous albitization in the Pyrenees: evidence from in situ U-Th-Pb dating of monazite, titanite and zircon. *Journal of the Geological Society* 167: 751–767.

Powers MC. 1953. A new roundness scale for sedimentary particles. *Journal of Sedimentary Research* 23: 117–119.

Ravier J. 1959. Le métamorphisme des terrains secondaires des Pyrénées. *Mem. Soc. Geol. Fr.* 1: 250.

Ribes C, Ghienne J-F., Manatschal G, Decarlis A, Karner GD, Figueredo PH, Johnson CA. 2019. Long-lived mega fault-scarps and related breccias at distal rifted margins: insights from present-day and fossil analogues. *Journal of the Geological Society* 176: 801–816. https://doi.org/10.1144/jgs2018-181.

Rokach L, Maimon O. 2005. Clustering methods. In: Maimon O, Rokach L, eds. *Data Mining and Knowledge Discovery Handbook*. Boston, MA: Springer, pp. 321–352.

Rossi P. 2002. The Pyrenean "Danian revolution". *Comptes Rendus Geoscience* 334: 583–584. https://doi.org/10.1016/S1631-0713(02)01790-X.

Roure F, Choukroune P, Berastegui X, Munoz JA, Villien A, Matheron P, Bareyt M, Seguret M, Camara P, Deramond J. 1989. Ecors deep seismic data and balanced cross sections: Geometric constraints on the evolution of the Pyrenees. *Tectonics* 8: 41–50.

Salardon R, Carpentier C, Bellahsen N, Pironon J, France-Lanord C. 2017. Interactions between tectonics and fluid circulations in an inverted hyper-extended basin: Example of mesozoic carbonate rocks of the western North Pyrenean Zone (Chaînons Béarnais, France). *Marine and Petroleum Geology* 80: 563–586.

Sapin F, Ringenbach J-C., Clerc C. 2021. Rifted margins classification and forcing parameters. *Sci Rep* 11: 8199. https://doi.org/10.1038/s41598-021-87648-3.

Shukla MK, Sharma A. 2018. A brief review on breccia: it's contrasting origin and diagnostic signatures. *Solid Earth Sciences* 3: 50–59.

Siron G, Goncalves P, Marquer D, Pierre T, Paquette J, Vanardois J. 2020. Contribution of magmatism, partial melting buffering and localized crustal thinning on the late Variscan thermal structure of the Agly massif (French Pyrenees). *J. Metamorph. Geol.* 38: 799–829.

Souquet P, Debroas E-J., Peybernes B, Boirie J-M., Pons P, Fixari G, Roux J-C., Dol J, Thieuloy J-P., Bonnemaison M, Manivit H. 1985. Le groupe du flysch noir (Albo-Cebomanien) dans les Pyrénées. *Bull. cent. rech. explor.- Prod. Elf-Aquitaine* 9: 183–252.

Stanton RJ. 1966. The Solution Brecciation Process. *Geol Soc America Bull* 77: 843.

Stewart IS, Hancock PL. 1990. Brecciation and fracturing within neotectonic normal fault zones in the Aegean region. *Geological Society, London, Special Publications* 54: 105–110.

Stewart IS, Hancock PL. 1988. Normal fault zone evolution and fault scarp degradation in the Aegean region. *Basin Research* 1: 139–153.

Sutra E, Manatschal G. 2012. How does the continental crust thin in a hyperextended rifted margin? Insights from the Iberia margin. *Geology* 40: 139–142.

Takahashi T. 1981. Debris Flow. *Annual Review of Fluid Mechanics* 13: 57–77.

Teixell A. 1998. Crustal structure and orogenic material budget in the west central Pyrenees. *Tectonics* 17: 395–406.

Teixell A, Labaume P, Lagabrielle Y. 2016. The crustal evolution of the west-central Pyrenees revisited: Inferences from a new kinematic scenario. *Comptes Rendus Geoscience, From rifting to mountain building: the Pyrenean Belt* 348: 257–267.

Ternois S, Odlum M, Ford M, Pik R, Stockli D, Tibari B, Vacherat A, Bernard V. 2019. Thermochronological evidence of early orogenesis, eastern Pyrenees, France. *Tectonics* 38: 1308–1336.

Ternois S, Mouthereau F, Jourdon A. 2021. Decoding low-temperature thermochronology signals in mountain belts: modelling the role of rift thermal imprint into continental collision. *BSGF – Earth Sci Bulletin* 192: 38.

Thiébaut J, Debeaux M, Durand-Wackenheim C, Souquet P, Gourinard Y, Bandet Y, Fondecave-Wallez M-J. 1988. Métamorphisme et halocinèse crétacés dans les évaporites de Betchat le long du Chevauchement Frontal Nord-Pyrénéen (Haute-Garonne et Ariège, France). *C. R. Acad. Sci., Sér. 2, Méc. Phys. Chim. Sci. Univers Sci. Terre* 307: 1535–1540.

Tournaire Guille B, Olivier Ph, Paquette J-L, Bosse V, Guillaume D. 2019. Evolution of the middle crust of the Pyrenees during the Paleozoic: new data on the plutonic rocks from the North Pyrenean Agly Massif. *Int J Earth Sci (Geol Rundsch)* 108: 245–265.

Tugend J, Manatschal G, Kusznir NJ, Masini E. 2015. Characterizing and identifying structural domains at rifted continental margins: application to the Bay of Biscay margins and its Western Pyrenean fossil remnants. *Geological Society, London, Special Publications* 413: 171–203.

Vacherat A, Mouthereau F, Pik R, Bernet M, Gautheron C, Masini E, Le Pourhiet L, Tibari B, Lahfid, A. 2014. Thermal imprint of rift-related processes in orogens as recorded in the Pyrenees. *Earth and Planetary Science Letters* 408: 296–306.

Vacherat A, Mouthereau F, Pik R, Bellahsen N, Gautheron C, Bernet M, Daudet M, Balansa J, Tibari B, Jamme RP, Radal J. 2016. Rift-to-collision transition recorded by tectonothermal evolution of the northern Pyrenees. *Tectonics* 35: 907–933.

Vanardois J, Trap P, Goncalves P, Marquer D, Gremmel J, Siron G, Baudin T. 2020. Kinematics, deformation partitioning and late Variscan magmatism in the Agly Massif, Eastern Pyrenees, France. *BSGF – Earth Sci. Bull.* 191: 15.

Vauchez A, Clerc C, Bestani L, Lagabrielle Y, Chauvet A, Lahfid A, Mainprice D. 2013. Preorogenic exhumation of the North Pyrenean Agly Massif (Eastern Pyrenees-France). *Tectonics* 32: 95–106.

Warren J. 2006. Karst, breccia, nodules and cement: Pointers to vanished evaporites. In: *Evaporites: sediments, resources and hydrocarbons*.

Woodcock NH, Mort K. 2008. Classification of fault breccias and related fault rocks. *Geol. Mag.* 145: 435–440.

Cite this article as: Motus M, Nardin E, Mouthereau F, Denèle Y. 2022. Evolution of rift-related cover-basement decoupling revealed by brecciation processes in the eastern Pyrenees, *BSGF - Earth Sciences Bulletin* 193: 14.